The Journal of Clinical Investigation

A selective microRNA-based strategy inhibits restenosis while preserving endothelial function

Gaetano Santulli,[1] Anetta Wronska,[1] Kunihiro Uryu,[2] Thomas G. Diacovo,[3] Melanie Gao,[1] Steven O. Marx,[4,5] Jan Kitajewski,[6] Jamie M. Chilton,[7] Kemal Marc Akat,[8] Thomas Tuschl,[8] Andrew R. Marks,[1,4] and Hana Totary-Jain[1,7]

[1]Department of Physiology and Cellular Biophysics, The Clyde and Helen Wu Center for Molecular Cardiology, Columbia University Medical Center, New York, New York, USA. [2]Electron Microscopy Resource Center, The Rockefeller University, New York, New York, USA. [3]Department of Pediatrics, [4]Department of Medicine, [5]Department of Pharmacology, and [6]Departments of Pathology and Obstetrics and Gynecology, Columbia University Medical Center, New York, New York, USA. [7]Department of Molecular Pharmacology and Physiology, Morsani College of Medicine, University of South Florida, Tampa, Florida, USA. [8]Howard Hughes Medical Institute and Laboratory for RNA Molecular Biology, The Rockefeller University, New York, New York, USA.

Drugs currently approved to coat stents used in percutaneous coronary interventions do not discriminate between proliferating vascular smooth muscle cells (VSMCs) and endothelial cells (ECs). This lack of discrimination delays reendothelialization and vascular healing, increasing the risk of late thrombosis following angioplasty. We developed a microRNA-based (miRNA-based) approach to inhibit proliferative VSMCs, thus preventing restenosis, while selectively promoting reendothelialization and preserving EC function. We used an adenoviral (Ad) vector that encodes cyclin-dependent kinase inhibitor p27^{Kip1} (p27) with target sequences for EC-specific miR-126-3p at the 3′ end (Ad-p27-126TS). Exogenous p27 overexpression was evaluated in vitro and in a rat arterial balloon injury model following transduction with Ad-p27-126TS, Ad-p27 (without miR-126 target sequences), or Ad-GFP (control). In vitro, Ad-p27-126TS protected the ability of ECs to proliferate, migrate, and form networks. At 2 and 4 weeks after injury, Ad-p27-126TS–treated animals exhibited reduced restenosis, complete reendothelialization, reduced hypercoagulability, and restoration of the vasodilatory response to acetylcholine to levels comparable to those in uninjured vessels. By incorporating miR-126-3p target sequences to leverage endogenous EC-specific miR-126, we overexpressed exogenous p27 in VSMCs, while selectively inhibiting p27 overexpression in ECs. Our proof-of-principle study demonstrates the potential of using a miRNA-based strategy as a therapeutic approach to specifically inhibit vascular restenosis while preserving EC function.

Introduction

Percutaneous coronary intervention (PCI) has transformed the treatment of coronary artery disease (CAD) (1–3). The major drawback of this procedure is restenosis, which is caused by intimal hyperplasia triggered during arterial wall injury with concurrent endothelial denudation (4). Restenosis primarily results from the proliferation and migration of vascular smooth muscle cells (VSMCs) into the intima, eventually leading to renarrowing of the lumen (4, 5). Previous studies demonstrated that sirolimus (rapamycin), a macrocyclic triene antibiotic (6, 7), inhibits VSMC proliferation and migration by inhibiting the downregulation of p27^{Kip1} (p27), a well-established cell-cycle regulator (8, 9). Such a discovery led to the development of the first sirolimus-coated stents. These drug-eluting stents (DES), quickly followed by other devices capable of delivering in situ antiproliferative agents (known as first- and second-generation DES), significantly reduced the clinical incidence of restenosis in comparison with

bare-metal stents (BMS), revolutionizing the field of PCI (3, 10). However, all drugs currently approved to coat DES do not discriminate between proliferating VSMCs and endothelial cells (ECs), thus delaying reendothelialization and subsequent vascular healing (11–15). This lack of drug specificity has greatly increased the risk of neoatherosclerosis and late thrombosis, potentially catastrophic events primarily caused by incomplete endothelial coverage of the treated vessel (15–18). These noteworthy health risks unfortunately require patients to endure prolonged regimens of dual-antiplatelet therapy following PCI (3, 19). A functional endothelium is critical for the regulation of vascular tone, suppression of intimal hyperplasia, neoatherosclerosis, and thrombi formation, and the reduction of dual-antiplatelet regimens (16, 20). Accordingly, an ideal therapy would selectively inhibit VSMC proliferation without affecting EC function (21). In this study, we investigated whether a microRNA-based (miRNA-based) strategy could be used as a selective therapy, inhibiting VSMC proliferation and hence neointimal hyperplasia, while simultaneously promoting vessel reendothelialization and preservation of EC function.

The discovery of miRNAs, a class of endogenous, small noncoding RNAs, represents a crucial breakthrough in the study of gene regulation. MiRNAs use base pairing to direct RNA-induced silencing complexes to specific mRNA transcripts containing partially or fully complementary sequences, resulting in the degradation or translational inhibition of the target

mRNA. They are active in most biological processes, including neointimal formation (22–24), and are expressed in tissue- and cell-specific patterns. In particular, miR-126, a pivotal regulator of vascular integrity and angiogenesis, is highly expressed in ECs (25, 26). MiR-126 is encoded within the seventh intron of the EC-specific gene epidermal growth factor–like domain 7 (*Egfl7*), which is critical for blood vessel formation and is upregulated in arterial injury sites and atherosclerotic plaques (27). The precursor miRNA pre–miR-126 is cleaved into 2 mature strands, miR-126-3p and miR-126-5p, two of the most abundant miRNAs in ECs (25, 26). Notably, lack of miR-126-5p, but not miR-126-3p, has been recently shown to impair endothelial recovery after denudation in *Mir126*$^{-/-}$ mice (26).

Endogenous miRNAs are remarkably effective in regulating transgene expression when tagged with artificial miRNA target sequences, according to the activity of the given miRNA (28, 29). In this study, we took advantage of the EC-specific miR-126 to design a unique adenoviral (Ad) vector, encoding the cell-cycle inhibitor p27 and incorporating 4 complementary target sequences for the mature miR-126-3p strand at its 3′ end (Ad-p27-126TS). Our aim was to overexpress exogenous p27, yet effectively regulate its overexpression in a cell-specific manner with the incorporated EC-specific miR-126-3p target sequences. Consequently, we hypothesized that exogenous p27 overexpression would be permitted in VSMCs, but not ECs, enhancing the degree of reendothelialization and restoration of EC function following injury. To evaluate our strategy, we quantified the effects of p27 overexpression with and without miR-126-3p target sequences on the proliferation and migration of VSMCs and ECs, as well as network formation and platelet aggregation in ECs. We further examined the in vivo effects of our approach on neointimal formation, surface reendothelialization, hypercoagulability, and EC function in a rat model of arterial balloon injury. Our results demonstrate that adding miR-126-3p target sequences to the 3′ end of exogenous *p27* not only selectively protects ECs from p27 overexpression, but also allows for complete reendothelialization and preservation of EC function in vivo. This initial proof-of-principle study provides the first step toward a novel therapeutic strategy to improve vascular healing and prevent late thrombosis following PCI.

Results

A unique Ad vector incorporating miR-126-3p target sequences selectively protects ECs from the antiproliferative and antimigratory effects of exogenous p27. Since we sought to leverage the EC-specific pattern of miR-126-3p expression, we first assessed the expression level of endogenous miR-126-3p in primary ECs and in VSMCs by real-time quantitative PCR (RT-qPCR). ECs showed greater than 600-fold higher expression of miR-126-3p compared with that detected in VSMCs (Figure 1A). To selectively overexpress exogenous p27 in VSMCs and not ECs, we designed the following Ad vectors, as illustrated in Figure 1B: (a) Ad-p27, a *p27* expression cassette driven by a CMV promoter; (b) Ad-p27-126TS, a p27 expression cassette driven by a CMV promoter containing 4 tandem copies of a 22-bp target sequence perfectly complementary to the mature miR-126-3p strand at the 3′ end of *p27*; (c) Ad-GFP, a control CMV-GFP Ad vector. All 3 vectors contained GFP under the control of a CMV promoter.

Next, we transduced primary human ECs and VSMCs (30 PFU/cell) with the 3 Ad vectors to assess protein expression levels of p27, GFP (to evaluate transduction efficiency), and GAPDH (loading control). Immunoblot analysis revealed that p27 was highly overexpressed in VSMCs and ECs transduced with Ad-p27 (Figure 1C). VSMCs, which express very low levels of endogenous miR-126-3p, showed high overexpression of p27 after transduction with Ad-p27-126TS (Figure 1C). Conversely, in ECs transduced with Ad-p27-126TS, we found that p27 overexpression was diminished, most likely due to endogenous endothelial miR-126-3p binding to its 4 target sequences at the 3′ end of the exogenous *p27* transcript, thereby leading to its degradation and/or inhibition of translation (Figure 1C). To ensure that the 4 target sequences for miR-126-3p did not act as "sponges" for endogenous miR-126-3p or its sister strand miR-126-5p, we transduced ECs with a higher number of particles (50 PFU/cell) of each of the 3 Ad vectors, and we assessed endogenous miR-126-3p and miR-126-5p levels as well as the miR-126-3p target gene *PIK3R2* by RT-qPCR (30). In Ad-p27–transduced ECs, miR-126-3p expression levels were comparable to those in Ad-GFP–transduced cells, whereas Ad-p27-126TS–transduced ECs exhibited a slight reduction (~20%) in endogenous miR-126-3p expression (Supplemental Figure 1A; supplemental material available online with this article; doi:10.1172/JCI76069DS1). We observed no significant differences in expression levels of *PIK3R2* (Supplemental Figure 1B) or miR-126-5p (Supplemental Figure 1C) among ECs transduced with the 3 Ad vectors. These results are in agreement with previous reports showing that 4 tandem repeat copies of a single target element are effective in the silencing of gene expression, while concurrently minimizing the saturation of miRNAs (28, 31–33).

Since Ad-p27-126TS led to an overexpression of p27 in VSMCs but not ECs, we tested whether Ad-p27-126TS would consequently inhibit VSMC proliferation without affecting ECs. Ad-p27 inhibited the proliferation of both cell types by more than 70% (Figure 1D). Importantly, the proliferation of VSMCs transduced with Ad-p27-126TS was also inhibited by more than 70%, whereas EC proliferation was unchanged (Figure 1D). Similarly, we tested the effect of transduction with the 3 Ad vectors on the migration of VSMCs and ECs in a wound-scratch assay. VSMCs and ECs transduced with Ad-p27 displayed greater than 75% inhibition of migration (Figure 2, A and B). Interestingly, transduction with Ad-p27-126TS led to the inhibition of VSMC migration by more than 70%, while EC migration was not inhibited (Figure 2, A and B). Then, we examined EC behavior following transduction using a network formation assay. ECs transduced with Ad-p27 displayed a marked decrease in network-like formation, whereas Ad-p27-126TS–transduced ECs formed networks comparable to those observed in ECs transduced with control Ad-GFP (Figure 2C). Finally, we performed a platelet adhesion assay to test the integrity of ECs and their antithrombotic phenotype in vitro. Compared with Ad-GFP, ECs transduced with Ad-p27 displayed a significant increase in platelet aggregation, while ECs transduced with Ad-p27-126TS showed minimal levels of platelet adhesion (Figure 2D).

Taken together, these data demonstrate that by inserting 4 target sequences for the EC-specific miR-126-3p at the 3′ end of *p27*, it is possible to overexpress exogenous p27 in VSMCs and thereby inhibit their capacity for proliferation and migration. Meanwhile,
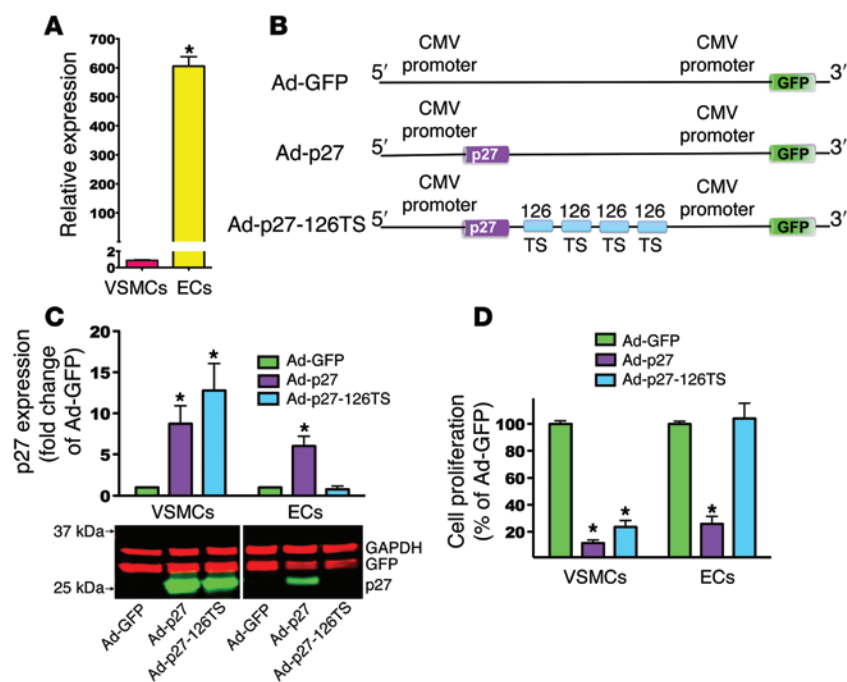
Figure 1. miR-126-3p target sequences selectively protect ECs from the antiproliferative effects of p27. (**A**) RT-qPCR analysis of miR-126-3p expression. (**B**) Schematic representation of the p27 expression cassette in the Ad vectors engineered to inhibit overexpression of exogenous p27 in cells expressing miR-126-3p (i.e., ECs). (**C**) Representative immunoblot of p27 protein expression from 3 independent experiments accompanied by densitometric quantification. Lanes were run on the same gel but were noncontiguous. For each cell type, p27 expression was normalized to each vector's GFP expression to account for transduction efficiency. (**D**) Proliferation assays of VSMCs and ECs transduced with the indicated Ad vector. Data represent the mean ± SEM of at least 3 experiments performed in quadruplicate. Data comparisons were made using 1-way ANOVA with Tukey-Kramer's post hoc test. *$P < 0.01$ versus VSMCs (**A**); *$P < 0.01$ versus Ad-GFP (**C** and **D**).

ECs displayed a nonthrombogenic phenotype, with preserved ability to proliferate, migrate, and form network-like structures.

Ad-p27-126TS inhibits neointimal formation in vivo. To test our approach in vivo, we used the rat carotid artery balloon injury model, transducing the vessel with the 3 different Ad vectors (34). Since the arterial wall heals within 28 days following stent implantation in animal models (4), we assessed the efficacy of our approach at 2 and 4 weeks after injury. Ad transduction efficiency was evaluated by GFP immunostaining of arterial sections using a Cy3-conjugated antibody. All arteries transduced with Ad-GFP, Ad-p27, or Ad-p27-126TS were GFP positive (Supplemental Figure 2, A and B). These findings are consistent with previous reports showing GFP expression in vivo 2 and 4 weeks after Ad transduction (35). To ascertain that Ad transduction was localized to the injury sites of the right carotid arteries and did not spread systemically, we performed GFP immunostaining of sections of the contralateral carotid artery. These sections were negative for GFP expression (Supplemental Figure 2A, uninjured). Moreover, we verified p27 overexpression in the carotid wall by immunoblot analysis of the vessel 3 days after transduction (Supplemental Figure 3). These data indicate that the in vivo Ad-mediated transductions were efficient and localized to the injured vessels.

Ad-mediated overexpression of p27 in balloon-injured arteries has been shown to inhibit restenosis (36, 37). To test whether Ad-p27-126TS would have comparable inhibitory effects on neointimal formation in vivo, we determined the intima/media ratios in carotid arteries 2 and 4 weeks after injury. We found that carotid arteries transduced with Ad-GFP exhibited a significant increase in the intima/media ratio compared with that in uninjured control vessels (Figure 3A and Supplemental Figure 4). Notably, transduction with both Ad-p27 and Ad-p27-126TS inhibited neointimal formation to a similar degree (Figure 3A and Supplemental Figure 4). Immunostaining for α-smooth muscle actin (α-SMA) confirmed that the neointima was primarily

composed of VSMCs (Figure 3B). Further staining for collagen and elastin in Ad-p27– and Ad-p27-126TS–transduced vessels indicated that p27 overexpression resulted in no undesirable fundamental alteration in the arterial structure (Supplemental Figure 5, A and B). These data indicate that both Ad-p27 and Ad-p27-126TS inhibited neointimal formation in vivo.

Ad-p27-126TS restores reendothelialization. We and others have previously demonstrated that overexpression of exogenous p27 inhibits not only VSMC, but also EC proliferation and migration (38, 39). Here, we assessed the endothelial integrity of carotid arteries injured and transduced with the 3 Ad vectors. EC-specific VE-cadherin (40) immunostaining was performed in longitudinal en face arterial preparations at 2 (Figure 4 and Supplemental Videos 1–4) and 4 weeks after injury (Supplemental Figure 6 and Supplemental Videos 5–7). The negative control (secondary antibody only) is depicted in Supplemental Figure 7 and Supplemental Video 8. Tridimensional evaluation revealed that Ad-GFP–transduced vessels displayed an irregular neointimal surface, presumably due to the severe restenotic process, with uneven endothelial coverage (Figure 4, A–D, Supplemental Figure 6, A and B, and Supplemental Videos 1, 2, and 5). Neither Ad-p27– nor Ad-p27-126TS–transduced arteries exhibited restenosis (Figure 4, E–H, Supplemental Figure 6, C–F, and Supplemental Videos 3, 4, 6, and 7). Strikingly, while Ad-p27–transduced vessels exhibited incomplete reendothelialization 2 and 4 weeks after injury (26% and 29% coverage compared with uninjured controls, respectively), Ad-p27-126TS–transduced vessels displayed extensive, uniform endothelial coverage (80% and 88%, respectively), as shown in Figure 4, G–I, and Supplemental Figure 6, E–G. These results were confirmed by scanning electron microscopy, showing a completely irregular internal surface in Ad-GFP–transduced vessels and a lack of endothelial coverage in Ad-p27–transduced vessels (Figure 4J), which displayed fibrotic remodeling that became more evident 4 weeks after injury (Supplemental Figure 6H). Conversely, transduction with

JCI
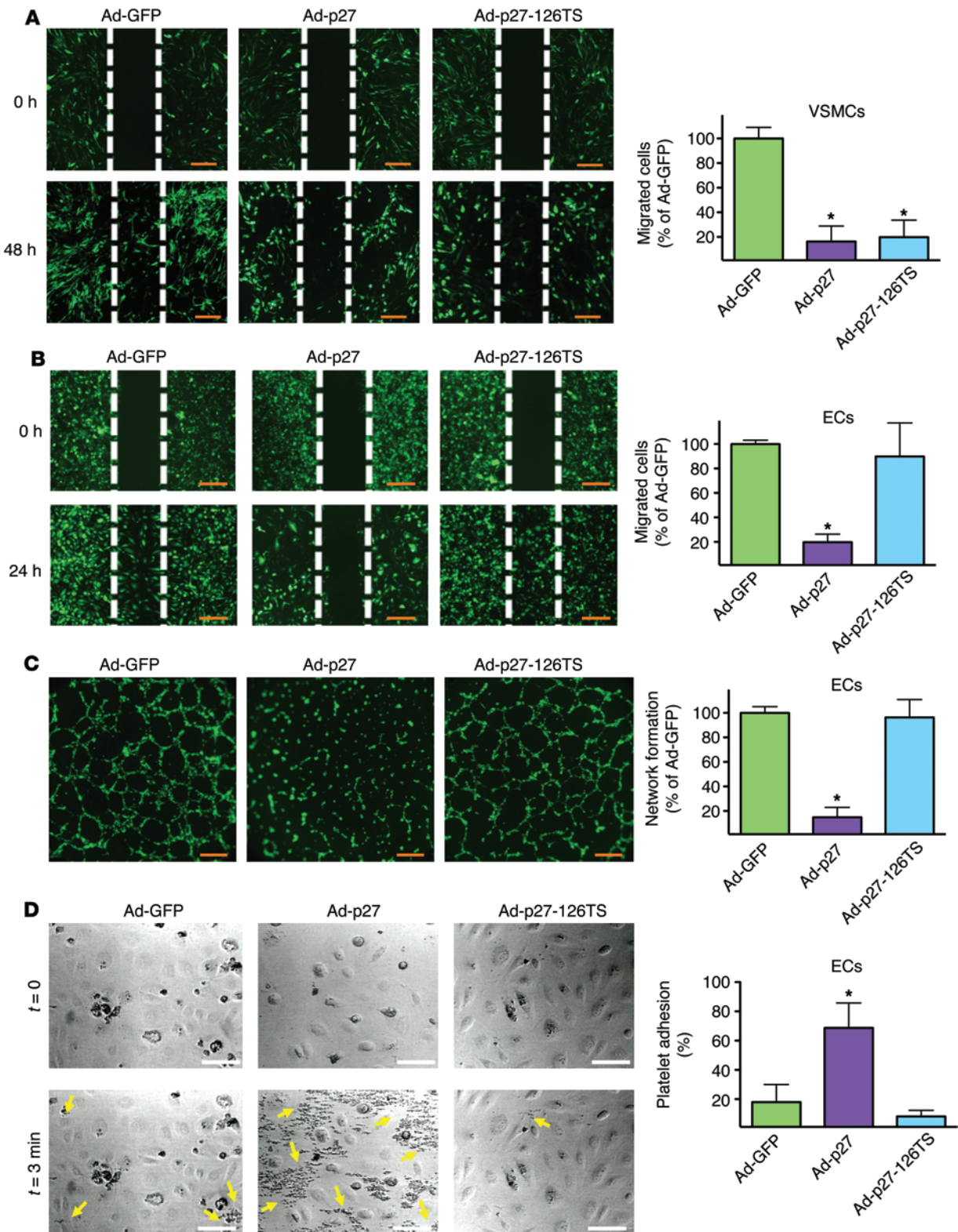
Figure 2. Ad-p27-126TS inhibits VSMC migration while preserving EC properties in vitro. Migration assays of VSMCs (**A**) and ECs (**B**) transduced with the indicated Ad vector. Representative images at the indicated time points are shown. Wound areas were measured using ImageJ64 software. (**C**) Formation of network-like structures in ECs was quantified by counting branch points. Scale bars: 100 μm (**A**–**C**). Data represent the means ± SEM of at least 3 experiments performed in quadruplicate. (**D**) Representative photomicrographs of platelet adhesion to ECs transduced with the indicated Ad vector in a parallel-plate flow chamber apparatus before (upper panels, *t* = 0) and after perfusion of PPACK-treated blood and washing (lower panels, *t* = 3 minutes). Yellow arrows represent human platelets. Scale bars: 30 μm. Graph on the right represents a quantification of the platelet adhesion test performed using Fiji software. Data represent the means ± SEM of at least 3 experiments performed in triplicate. Data comparisons were made using 1-way ANOVA with Tukey-Kramer's post hoc test. *$P < 0.01$ versus Ad-GFP.

Ad-p27-126TS preserved the reendothelialization process at both 2 (Figure 4J) and 4 weeks (Supplemental Figure 6H) after injury.

We further examined reendothelialization in cross sections of the carotid arteries by immunostaining for VE-cadherin. Uninjured control vessels exhibited distinct EC staining, whereas in Ad-GFP–transduced arteries, which had significant neointimal growth, the endothelium was only minimally detectable at both 2 and 4 weeks after injury (Figure 5, A and B, and Supplemental Figure 8, A and B). Ad-p27–transduced vessels also displayed diminished endothelial coverage (Figure 5, A and B, and Supplemental Figure 8, A and B). Crucially, in arteries transduced with Ad-p27-126TS, we observed a progressive and widespread reendothelialization (Figure 5, A and B, and Supplemental Figure 8, A and B). These data strongly support our in vitro findings (Figure 1D and Figure 2, A and B), demonstrating that overexpression of exogenous p27 inhibits both VSMC and EC proliferation and migration, whereas transduction with Ad-p27-126TS exclusively inhibits VSMC proliferation and migration but concurrently allows EC proliferation and migration, which may explain the reendothelialization observed in the injured vessels.

Finally, we assessed the arterial inflammatory state by immunostaining for CD45, a pan-inflammatory cell-surface marker present on all hematopoietic cells except erythrocytes and platelets. Both Ad-p27– and Ad-p27-126–treated vessels displayed a reduced arterial inflammatory response compared with that of uninjured controls, while we observed an intense inflammatory reaction in the adventitia of Ad-GFP–treated arteries (Supplemental Figure 9).

Ad-p27-126TS attenuates hypercoagulability in vivo. Since clinical and pathological studies have reported incomplete endothelial coverage after PCI leading to thrombosis (12), we assessed hypercoagulability by measuring plasma D-dimer levels before (uninjured) and 3, 14, and 28 days after injury and transduction with the Ad vectors. All treatments showed increased D-dimer levels at day 3, most likely in immediate response to injury (Figure 6A). Rats treated with Ad-GFP or Ad-p27 exhibited a significant increase in D-dimer levels at both 14 and 28 days after surgery (Figure 6A). Strikingly, in the rats treated with Ad-p27-126TS, which displayed complete inhibition of neointimal growth and complete reendothelialization, the D-dimer levels were comparable to those of the uninjured animals at both 14 and 28 days after injury (Figure 6A).

Ad-p27-126TS restores EC function after arterial balloon injury. To evaluate endothelial function, we performed vascular reactivity assays (20) using carotid rings harvested from rats 2 and 4 weeks after injury. Carotid arteries transduced with Ad-GFP exhibited markedly diminished vasodilatation in response to acetylcholine compared with that observed in uninjured vessels, most likely due to restenosis (Figure 6, B and C). Ad-p27–transduced vessels also displayed an impaired vasodilatory response (Figure 6, B and C). Intriguingly, arteries transduced with Ad-p27-126TS showed normal vasodilatation, comparable to that seen in uninjured control vessels at both 2 and 4 weeks after injury (Figure 6, B and C). We observed no significant difference in the endothelium-independent vasodilatory response to nitroprusside (Supplemental Figure 10). These data are consistent with our in vitro results and with the tridimensional confocal images and further confirm the integrity of the endothelium in Ad-p27-126–treated arteries.

Discussion

Clinical use of DES, with their controlled release of antiproliferative agents, has significantly reduced the incidence of restenosis following PCI in comparison with BMS use (3). However, their lack of drug specificity inhibits the proliferation and migration of both VSMCs and ECs in the vessel (11). While this nonselective drug action does inhibit neointimal hyperplasia, it effectively impairs the endothelial regeneration that is critical to vascular healing. Indeed, pathological studies have demonstrated that the delayed and insufficient reendothelialization common to both first- and second-generation DES directly contributes to objectionably high rates of uncovered struts, late thrombosis, and neoatherosclerosis (16, 41). The current study shows an innovative proof-of-principle approach to overcome the limitations and risks associated with currently available devices. We report here the first miRNA-based strategy to our knowledge to selectively inhibit VSMC proliferation and migration for the prevention of restenosis, without concurrently inhibiting reendothelialization and EC function. We uniquely leveraged EC-specific miR-126 to design an Ad vector containing target sequences complementary to the mature miR-126-3p strand at the 3′ end of *p27* in order to overexpress exogenous p27 in VSMCs, selectively preserving ECs. Our strategy is based on previous reports that indicated the feasibility of suppressing transgene expression up to 100-fold using properly engineered target sites for a highly expressed miRNA (28, 32). Therefore, we exploited the endogenous, tissue-specific expression of miR-126-3p without affecting the bioactivity of miR-126-5p reported in ECs (26).

To our knowledge, no previous evidence suggests that miR-126 is endogenously expressed in VSMCs. However, we cannot discount the recent findings that miR-126 is secreted by ECs and transferred to VSMCs (42). Even so, the reported levels of transmitted miR-126 in VSMCs remained insufficiently low in both in vitro cocultures with ECs and in vivo shear stress conditions to impede our strategy. Nevertheless, to validate our approach, we first confirmed the lack of endogenous miR-126-3p expression in VSMCs and its endothelial specificity. We assessed the level of endogenous miR-126-3p via RT-qPCR and found it to be 600-fold higher in ECs compared with the levels detected in VSMCs in vitro. This significant difference strengthened our assumption that the level of endogenous miR-126-3p expression displayed by ECs was sufficient to bind the target sequences introduced by the Ad vector and effectively inhibit exogenous p27 overexpression and its effects on ECs. Conversely, VSMCs lacking endogenous miR-126-3p permitted overexpression of exogenous p27.

In healthy arteries, p27 is constitutively expressed in quiescent VSMCs (5). As a member of the Cip/Kip family of cyclin-dependent kinase (CDK) inhibitors, p27 binds and modulates cyclin D–, E– and A–dependent kinases, resulting in G_1/S transition failure and cell-cycle arrest (5). The inhibitory effects of p27 in the arterial wall have been shown to be more potent than those of other members of the CDK inhibitors, including p21[Cip1] and p16[Ink4] (37). Upon vascular injury, however, multiple response mechanisms are initiated, and the entry of activated VSMCs into the cell cycle represents the final common pathway, in which p27 is rapidly downregulated, enabling VSMCs to resume cell divi-
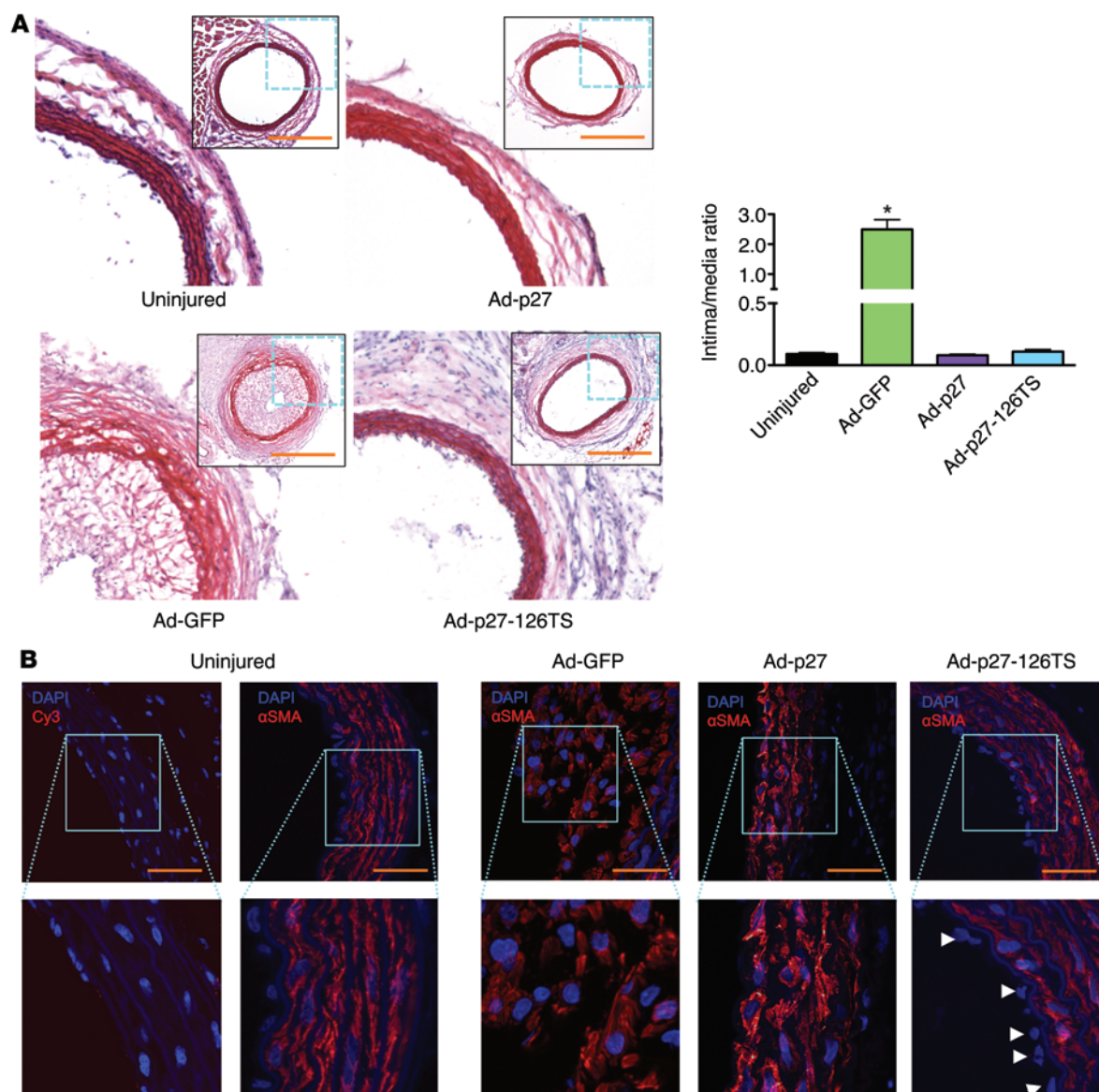
Figure 3. Ad-p27 and Ad-p27-126TS inhibit restenosis 2 weeks after balloon injury. (A) Representative H&E-stained sections. Scale bars: 500 μm; original magnification, ×10 (insets show the whole arterial section at ×5 original magnification). Intima/media ratios were calculated from at least 6 rats/group. Data represent the means ± SEM. Data comparisons were made using 1-way ANOVA with Tukey-Kramer's post hoc test. *$P < 0.01$ versus uninjured arteries. **(B)** Representative sections of rat carotid arteries immunostained for α-SMA. Nuclei were counterstained with DAPI. No positive staining was observed in the negative control sections. Scale bars: 100 μm; original magnification, ×60 and ×120 (insets). Arrowheads indicate EC nuclei beyond the inner autofluorescent elastic laminae.

sion, thereby triggering intimal hyperplasia and leading to vascular restenosis (4). The clinical importance of a single nucleotide polymorphism in the *p27* gene, which has been associated with an increased risk of myocardial infarction, underlies the central role of p27 in the pathophysiology of vascular remodeling (43). Overexpression of exogenous p27 in VSMCs has been demonstrated to result in G_1 phase arrest, leading to a significant reduction of neointimal formation in a porcine femoral arterial injury model (37). In contrast, *p27*-knockout mice displayed a significant increase in VSMC proliferation and developed extensive arterial lesions (44). Furthermore, previous studies specifically evaluating the role of p27 overexpression in a rat carotid model of balloon angioplasty, like the one used here, demonstrated that the upregula-

tion of p27 led to VSMC growth arrest and attenuated neointimal lesion formation (36). Several reports have also demonstrated that sirolimus, clinically used in DES coating (1, 11, 14), blocks the degradation of p27, thereby preventing VSMC proliferation and migration (5, 8). In particular, sirolimus treatment produces an increase in p27 by reducing p27-targeted degradation by phosphorylation at Thr187 (5, 8). Thus, both p27 overexpression and sirolimus treatment strategies eventually result in the upregulation of p27 expression (although along different pathways) to control VSMC cell-cycle behavior, making exogenous p27 overexpression a means to broadly mimic treatment with sirolimus or its analogs used in DES. Importantly, the antiproliferative and antimigratory effects of sirolimus, eventually mediated by p27,
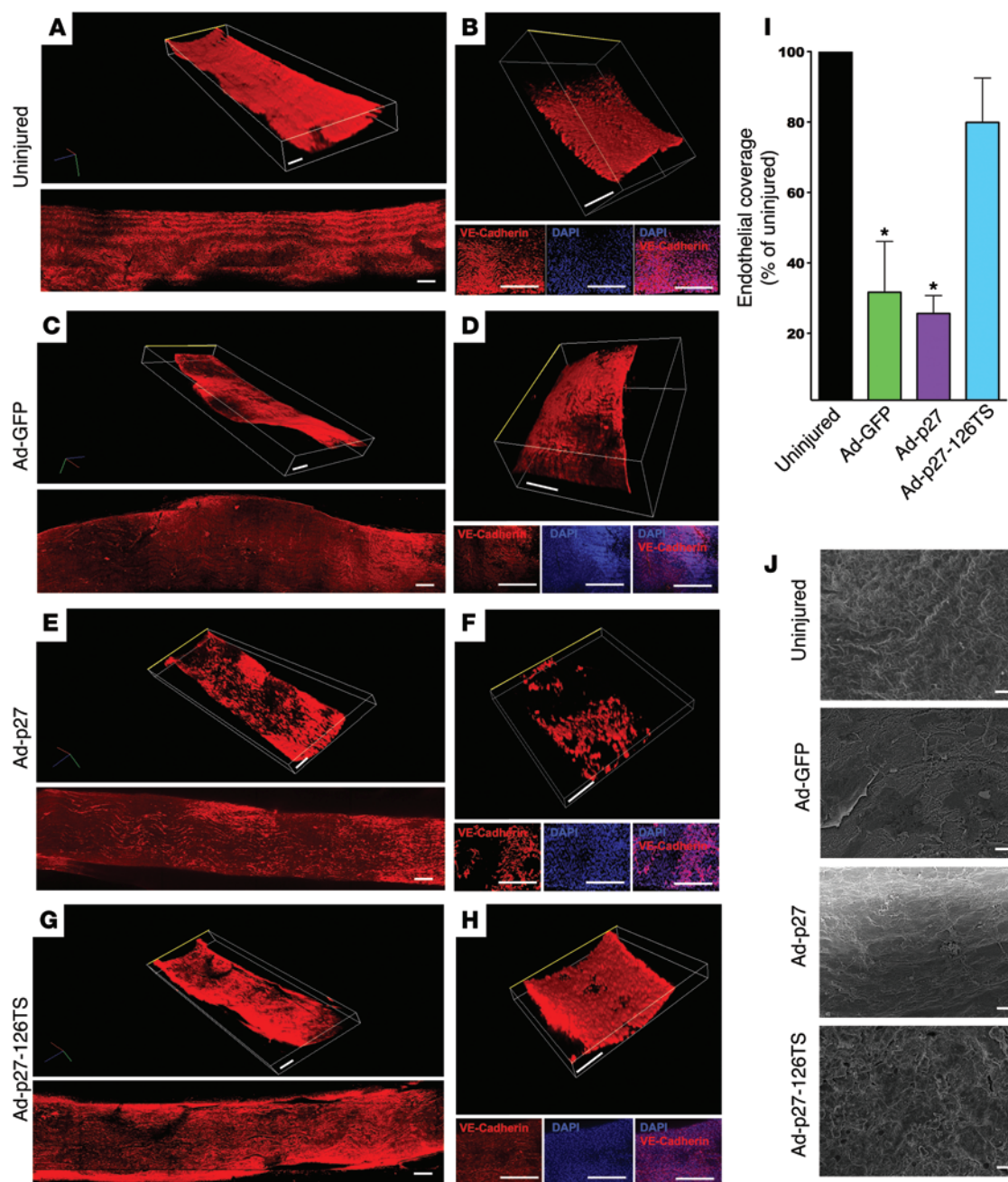
Figure 4. Ad-p27-126TS restores endothelial coverage of en face longitudinal arterial preparations. (**A**–**H**) Representative confocal images of the internal surface of the vessels immunostained for VE-cadherin. (**A**, **C**, **E**, and **G**) Tridimensional (top) and bidimensional (bottom) images of the longitudinal en face preparation of the carotid arteries. (**B**, **D**, **F**, and **H**) Tridimensional images of a representative central portion (see Methods and Supplemental Figure 7A for detailed information about the imaging procedure) of the vessel (top), with the respective 2D pictures showing the EC-specific immunostaining for VE-cadherin (bottom: VE-cadherin, DAPI, and merge) and representing the endothelial coverage, which is quantified in **I**; the luminal side is indicated by a yellow line. See also the Supplemental Videos 1–4 for a tridimensional view. Dimensional scale bars: 400 μm (all 2D and 3D images). Data comparisons were made using 1-way ANOVA with Tukey-Kramer's post hoc test; n = at least 5/group. *$P < 0.01$ versus uninjured arteries. (**J**) Representative scanning electron microscopy images of the internal surface of uninjured, Ad-GFP–, Ad-p27–, and Ad-p27-126TS–transduced arteries. Scale bars: 10 μm.

are not exclusive to VSMCs, as they have also been previously observed in ECs (38, 39). We therefore speculated that exogenous p27 overexpression would affect both VSMCs and ECs. Our data are in agreement with the established mechanism of action of p27. When transduced with Ad-p27, which does not contain miR-126-3p target sequences, both VSMCs and ECs overexpressed p27 to a similar degree and exhibited similar behavior. In vitro, we found that exogenous p27 overexpression inhibited proliferation and migration of both VSMCs and ECs by ~70% and 75%, respectively, indicating that exogenous p27 overexpression has similar potency in regulating the cell cycle of VSMCs and ECs. In vivo, p27 overexpression inhibited neointimal formation.

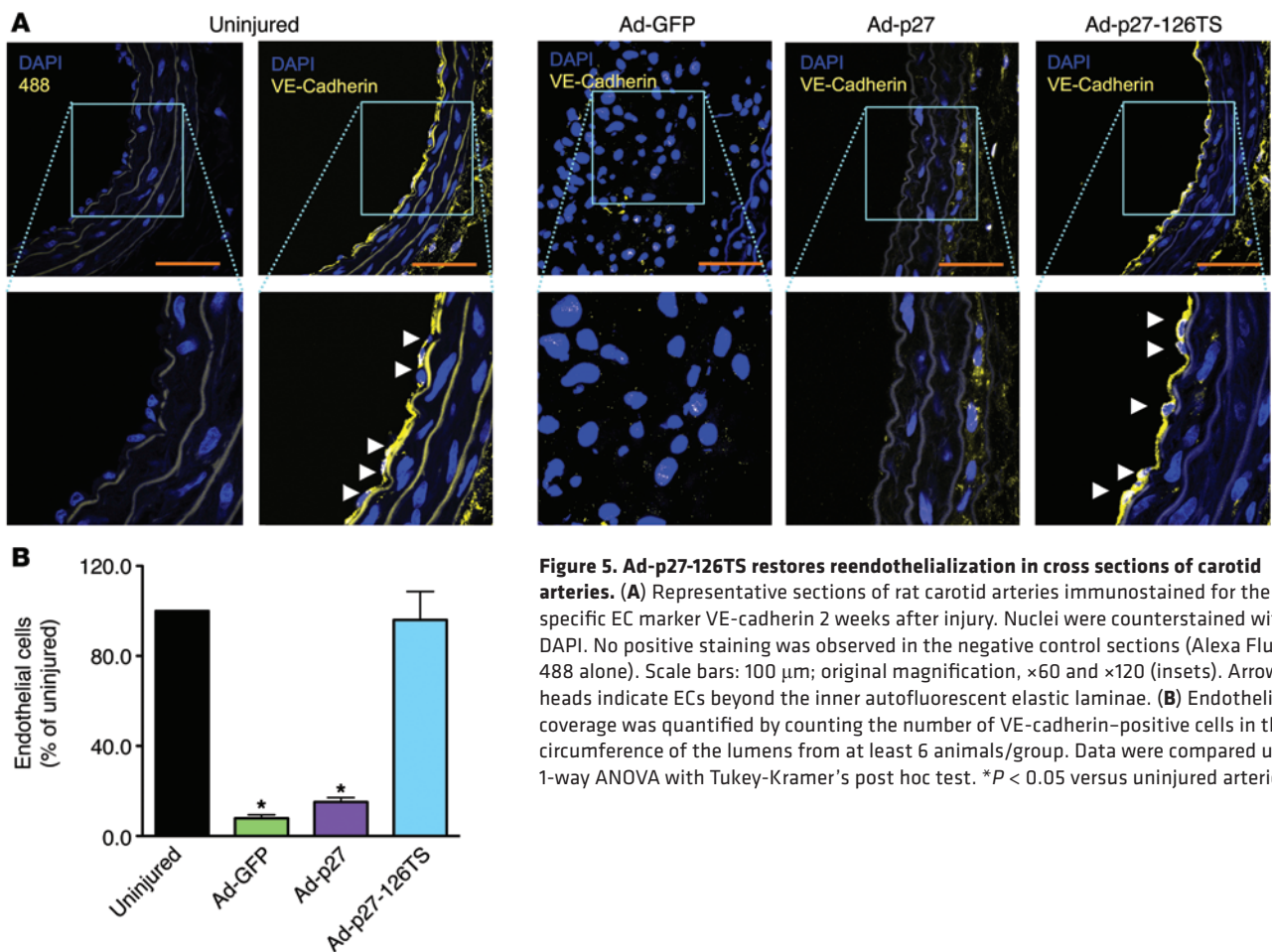**Figure 5. Ad-p27-126TS restores reendothelialization in cross sections of carotid arteries.** (**A**) Representative sections of rat carotid arteries immunostained for the specific EC marker VE-cadherin 2 weeks after injury. Nuclei were counterstained with DAPI. No positive staining was observed in the negative control sections (Alexa Fluor 488 alone). Scale bars: 100 μm; original magnification, ×60 and ×120 (insets). Arrowheads indicate ECs beyond the inner autofluorescent elastic laminae. (**B**) Endothelial coverage was quantified by counting the number of VE-cadherin–positive cells in the circumference of the lumens from at least 6 animals/group. Data were compared using 1-way ANOVA with Tukey-Kramer's post hoc test. *$P < 0.05$ versus uninjured arteries.

Although p27 overexpression beneficially inhibited restenosis, it significantly impaired reendothelialization and sustained hypercoagulability. Indeed, we found that exogenous p27 overexpression led to a prolonged inhibitory effect on reendothelialization (23% and 29% endothelial coverage in Ad-p27 vessels assessed at 2 and 4 weeks after injury, respectively). Consistently, D-dimer levels were significantly higher in Ad-p27–treated rats at 2 and 4 weeks after injury compared with levels in uninjured controls. In addition, Ad-p27–transduced vessels demonstrated significantly impaired endothelial function compared with that in uninjured controls. These results indicate that the inhibition of neointimal hyperplasia by overexpression of exogenous p27, without sparing ECs, fails to result in restoration of normal physiological function of the vessel after injury. These observations mirror the deleterious effects that current nonselective DES used in PCI have on ECs and vascular healing and are in accordance with the reported increased risk of thrombosis associated with DES when compared with BMS (3, 12, 45, 46).

The simple incorporation of 4 miR-126-3p target sequences within our Ad-p27-126TS vector profoundly modulated the response to exogenous p27 overexpression in ECs and provided robust EC protection. Incorporating target sequences for just the mature miR-126-3p strand was distinctly advantageous, since we could exploit the EC specificity of miR-126, yet our target sequences did not serve as a sponge to diminish the bioactivity

of miR-126-3p's sister strand miR-126-5p, which recent evidence confirmed as an essential player in promoting EC proliferation and preventing atherosclerotic lesion formation (26). Consequently, in vitro, ECs transduced with Ad-p27-126TS no longer demonstrated the antiproliferative and antimigratory effects of exogenous p27 expression. ECs exhibited preserved network formation and reduced platelet adhesion compared with cells overexpressing exogenous p27 (Ad-p27). The inhibition of exogenous p27 expression in the Ad-p27-126TS treatment group was so effective in vitro that EC proliferation, migration, network formation, and platelet adhesion were restored to levels comparable to those seen in controls (Ad-GFP). In vivo, we evaluated vascular response at 2 and 4 weeks after injury, the longer time course allowing for more extended evaluation of the endothelial repair. We found that neointimal hyperplasia was inhibited in the Ad-p27-126TS–treated vessels as effectively as in the Ad-p27–treated vessels at 2 and 4 weeks after injury due to the lack of endogenous miR-126 in VSMCs in both groups. Hence, according to our study, treatment with Ad-p27-126TS was as successful as Ad-p27 in preventing restenosis.

Remarkably, treatment with Ad-p27-126TS resulted in almost complete reendothelialization as soon as 2 weeks after injury (80%), in sharp contrast to Ad-p27 treatment, in which EC coverage remained below 30% even after 1 month. We speculate that the endothelial coverage is triggered by EC proliferation
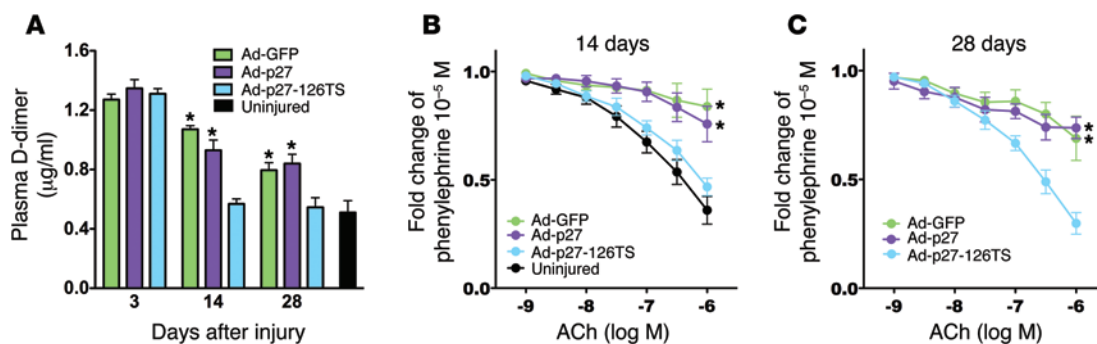
Figure 6. Ad-p27-126TS reduces hypercoagulability and restores EC function in vivo. (**A**) Plasma D-dimer levels evaluated before (uninjured) and 3, 14, and 28 days after balloon injury using a specific immunoassay. $n = 5$ animals/group. (**B** and **C**) Vascular reactivity analysis on carotid rings 2 (**B**) and 4 (**C**) weeks after injury showing the vasodilatory response to acetylcholine (ACh). $n = 5–6$ rats/group. Data represent the means ± SEM and were compared using 1-way (**A**) or 2-way repeated-measures (**B** and **C**) ANOVA followed by Tukey-Kramer's post hoc test. *$P < 0.01$ versus uninjured arteries.

miR-126 is enriched in ECs and upregulated in arterial injury sites and in atherosclerosis (27), we assume that exogenous p27 would be overexpressed in Ad-p27-126TS–transduced arteries in VSMCs and in all the cell types that do not express miR-126. In this sense, exogenous p27 overexpression ultimately inhibited the infiltration of inflammatory cells to the injured vessel.

and migration from sites adjacent to the injury. Endothelial progenitor cells might also play a role in the reendothelialization process, although this notion is still controversial (47, 48). In Ad-p27-126TS–treated rats, we observed that reendothelialization was accompanied by a sharp decrease in plasma D-dimer levels to those observed in uninjured control animals as early as 2 weeks after injury. In addition, treatment with Ad-p27-126TS not only reduced hypercoagulability compared with that seen in Ad-p27–treated rats, but restored the endothelium-dependent vasodilatory response to levels indistinguishable from those in uninjured controls. Therefore, our strategy not only reendothelialized injured vessels, but did so with functional ECs. This finding represents a major improvement over the current state-of-the-art devices used for PCI, since previous studies have demonstrated that improving reendothelialization without improving endothelial function is not enough to prevent late thrombosis (48). Given these results, reducing the need for prolonged dual antiplatelet therapy to prevent late thrombosis may be another welcome benefit to CAD patients should our miRNA-based strategy show efficacy in the clinical setting.

Moreover, the reendothelialization of vessels with functional ECs presented here may have implications for neoatherosclerosis. Several investigators have recently demonstrated that the inability to restore and maintain functional ECs following PCI increases the incidence of neoatherosclerosis in DES compared with BMS (15, 16, 41). Moreover, p27 has been shown to play a key role in atherosclerosis. Indeed, p27 deficiency leads to increased atherosclerotic plaque formation in *Apoe*$^{-/-}$ mice (49). Thus, we can also speculate that our strategy might prevent or inhibit neoatherosclerosis by targeting the cells involved in this process while preserving EC regeneration and promoting vessel healing. Further investigation is necessary to prove this particular concept, which is beyond the scope of the present study.

Another strength of this study is the assessment of inflammation, an important feature in the pathophysiology of restenosis (4). Our data are supported by previous reports showing that p27 directly regulates the proliferation of bone marrow–derived cells (hematopoietic and nonhematopoeitic) that migrate to damaged blood vessels and reconstitute vascular lesions (44). Since endogenous

For the experiments presented herein, we elected to use an Ad delivery vehicle in a rat model of balloon angioplasty, a common choice for studying restenosis (34, 50–53). We are indeed aware that stents were not used in our animal model, and the time course of neointimal growth and reendothelialization in rodents is more rapid than in humans, especially since healthy and juvenile animals normally heal within 28 days after injury (4, 54). Nevertheless, our experimental system was inexpensive and within our means, representing the most efficient approach to establishing proof-of-concept of our miRNA-based strategy without extensive design considerations. By eliminating variables introduced by disease models, choice of stent platform, strut thickness, and polymer coating (55), we focused on the direct effects on arterial injury resulting from exogenous p27 overexpression and incorporation of miR-126-3p target sequences.

However, to translate our miRNA-based strategy to a clinically relevant setting, we acknowledge that additional studies beyond the scope of this work will need to be conducted to assess its long-term efficacy and safety. For instance, late-generation adeno-associated viral (AAV) vectors could be used as an alternative delivery vehicle, reducing immune response concerns, and applied locally through gene-eluting stents or emerging nanotechnology-based scaffolds (21, 56). Different numbers of miR-126-3p target sequences may also be evaluated to better modulate exogenous p27 overexpression or to prevent miR-126-3p target sequences from acting as a sponge for endogenous miR-126-3p (57). Additionally, miR-126 target sequences could also be used to regulate the exogenous overexpression of alternative or additional genes of interest besides *p27*. Our miRNA-based strategy obviously needs to be evaluated within a stent platform as well as investigated in larger animal models. Ideally, future studies would be within the context of an atherosclerotic disease model. Indeed, an atherosclerotic animal model would allow us to evaluate whether the selective enhancement of reendothelialization and preserved EC function demonstrated by our miRNA-based strategy shows long-term protection against neoatherosclerosis and thrombosis. Therefore, our strategy could potentially combine the inhibition

of restenosis, inflammation, and neoatherosclerosis with the promotion of reendothelialization and vascular healing.

In summary, our findings demonstrate that it is feasible to use a miRNA-based strategy to combine antiproliferative and pro-healing mechanisms for enhanced arterial repair. Various therapeutic approaches have been designed to reduce neointimal hyperplasia, accelerate reendothelialization, or inhibit thrombosis. Our strategy has the potential to achieve all of these objectives in a single, comprehensive treatment. Moreover, this approach could be exploited across multiple conditions, including transplant vasculopathy, arteriovenous fistulae, and vein graft failure. The results presented here provide the basis for designing the next generation of selective therapy in PCI. The combination of a better stent platform and biodegradable polymer with this selective inhibition of VSMCs, without affecting ECs, has the potential to revolutionize the future of vascular interventional medicine.

Methods

Design of Ad vectors. Recombinant Ad vectors containing *p27* (Ad-p27) and *p27* with 4 tandem target sequences for hsa-miR-126-3p introduced at its 3′ end (Ad-p27-126TS) were constructed using AdEasy XL (Agilent Technologies) in accordance with the manufacturer's instructions. Briefly, *p27* was amplified with primers 5′-agtcggtaccacc**ATG**TCAAACGTGCGAGTGTCTAACGG-3′ and 5′-gatctgtacaggatcc**TTA**CGTTTGACGTCTTCTGAGGCC-3′ (start and stop codons are in bold and restriction sites in lowercase) and subcloned into a carrier vector. Complementary oligonucleotides containing 4 targeting sequences for miR-126-3p (in bold) (5′-aattcAT**CGCATTATTACTCACGGTACGA**AATC**CGCAT-TATTACTCACGGTACGA**AATC**CGCATTATTACTCAC-GGTACGA**AATC**CGCATTATTACTCACGGTACGA**ATg-3′ and 5′-aattcAT**TCGTACCGTGAGTAATAATGCG**GATT**TCG-TACCGTGAGTAATAATGCG**GATT**TCGTACCGTGAGTAA-TAATGCG**GATT**TCGTACCGTGAGTAATAATGCG**ATg-3′) were annealed and subcloned at the 3′ end of *p27* with EcoRI. Next, *p27* and *p27*-126-3pTSx4 were amplified from the carrier vector with the following pairs of primers: 5′-agtcggtaccacc**ATG**TCAAAC-GTGCGAGTGTCTAACGG-3′ as a sense primer for both constructs, and 5′-agtcctcgag**TTA**CGTTTGACGTCTTCTGAGGCC-3′ and 5′-agtcctcgagaTTCGTACCGTGAGTAATAATGCGGATTTC-3′ as antisense primers for *p27* and *p27*-126-3pTSx4, respectively. The resulting PCR products were subcloned into a pAdTrack-CMV shuttle vector (using Acc65 I and Xho I restriction sites, shown in lowercase) under the control of a CMV promoter. All the constructs also contained a GFP under the control of a CMV promoter. All final Ad constructs were confirmed by sequencing, purified by ultracentrifugation in CsCl gradient, dialyzed, and titrated in human embryonic kidney (HEK) cells (58).

Cell culture. Human umbilical venous ECs were cultured in EGM2 Bullet Kit medium (Lonza Group) on dishes coated with type I rat tail collagen (VWR International). Human VSMCs and SmGM-2 Bullet Kit medium were purchased from Lonza Group. The cells in all assays were below passage 6 and cultured at a density that allowed cell division throughout the course of the experiments.

RT-qPCR. TaqMan microRNA Assays (Life Technologies, Thermo Fisher Scientific) were used to quantify mature miR-126-3p

and miR-126-5p as previously described (59). cDNA was synthesized by priming with miR-specific looped primers or by U18 as an endogenous control. For *GFP* and *GAPDH* expression analyses, 500 ng total RNA was used to synthesize cDNAs using M-MuLV reverse transcriptase (New England BioLabs) according to the manufacturer's specifications. All reactions, excluding no-template controls and non-reverse-transcribed controls, were run in triplicate and incubated in 96-well plates at 95°C for 20 seconds, followed by 40 cycles of 95°C for 3 seconds and 60°C for 30 seconds using the ABI 7500 Fast Real Time PCR Detection System. RT-qPCR data were analyzed using the comparative CT method and normalized to the expression of *U18* for miR-126-3p and miR-126-5p or *GAPDH* for *GFP* and *PIK3R2*.

Immunoblotting. Immunoblot analyses were performed as previously described (7, 35). Briefly, VSMCs and ECs were transduced with 30 PFU/cell. Samples were size fractionated by SDS-PAGE, and proteins were transferred to polyvinylidene difluoride membrane and visualized by immunoblotting using infrared-labeled anti-rabbit (red) and anti-mouse (green) secondary antibodies (1:10,000; LI-COR). Band intensities were quantified with the Odyssey Infrared Imaging System (LI-COR). The blots were probed with the following antibodies: rabbit anti-GAPDH (Cell Signaling Technology); rabbit anti-GFP (Life Technologies, Thermo Fisher Scientific); and mouse anti-p27 (BD Transduction Laboratories, BD Biosciences). Data are presented as arbitrary units after normalization to GAPDH as a loading control.

Proliferation, migration, and network formation assays. VSMCs and ECs were transduced with 20 or 30 PFU/cell, respectively. Proliferation assays were conducted 6 days after transduction using the Cell Proliferation Reagent kit (Roche Applied Science) according to the manufacturer's instructions. The absorbance was measured at 450 nm (with a 690-nm reference wavelength) using the Infinite F500 microplate reader (Tecan Group).

Cellular migration was assessed as previously described and validated (60, 61). Briefly, a confluent cell monolayer was scraped with a sterile pipette tip to generate a scratch wound and washed twice with medium to remove cell debris. Time-lapse images were captured at 0, 24 (ECs), and 48 hours (VSMCs). The wound areas were measured using ImageJ64 software (NIH). The formation of network-like structures assay was performed and quantified by counting branch points as previously described and then validated (60, 62). Several fields of view were captured per well, and experiments were repeated 3 times by blinded observers.

Platelet adhesion assay. Platelet adhesion was assessed in a parallel-plate flow chamber apparatus (GlycoTech) as previously described (63). Human venous whole blood samples were drawn into H-D-Phe-Pro-Arg-chloromethylketone (PPACK, 100 μM final concentration; EMD Millipore) to prevent coagulation. Whole blood (500 μl) was perfused at a wall shear rate of 1,600 s^{-1} over fibronectin-coated 6-well plates in which ECs had been cultured and transduced (30 PFU/cell) with Ad-GFP, Ad-p27, and Ad-p27-126TS for 5 days. Blood was perfused for 2 minutes, followed by washing with Tyrode's buffer under identical flow conditions for 1 minute. Platelet attachment was recorded on Hi-8 videotape using a TE2000 Nikon microscope with a phase-contrast ×20 objective. The areas covered by platelets were quantified using a computerized image analysis system (FIJI), including 4 fields of view for each data point.

Experimental animals and in vivo balloon injury. Balloon injury of the right carotid artery was performed in male Sprague-Dawley rats

(weighing 300 ± 35 g; Harlan Laboratories) using a HyperGlide balloon catheter (Micro Therapeutics) as previously described (34). The animals were anesthetized by isoflurane (4%) inhalation and maintained by mask ventilation (isoflurane 2%), and the right common, external, and internal carotid arteries were exposed and isolated. Through the external carotid artery, the balloon catheter was introduced into the common carotid artery and inflated 7 times. After injury, the common carotid artery was flushed twice with PBS, and a solution of PBS and Ad (5×10^9 PFU/100 μl) was injected and allowed to incubate in the common carotid artery in the absence of flow for 20 minutes. During this procedure, the tension of the common carotid artery was maintained by placing microvascular clips (Harvard Apparatus) on the internal and common carotid arteries (64). The Ad was then removed by aspiration. The external carotid artery was tied, and blood flow was restored through the common and internal carotid arteries. Following wound closure, the rats were given ad libitum access to food and water. The animals were housed in a 22°C room with a 12-hour light/12-hour dark cycle. All experiments were performed by blinded investigators.

D-dimer measurement. Hypercoagulability was assessed by measuring D-dimer plasma levels using a rat-specific ELISA Kit for D-dimer (USCN Life Science) according to the manufacturer's instructions.

Immunofluorescence. Two and 4 weeks after surgery, the rats were euthanized and perfused at 100 mmHg with 100 ml PBS, followed by 80 ml PBS containing 4% paraformaldehyde via a cannula placed in the cardiac left ventricle. For en face longitudinal arterial preparations, both right and left common carotid arteries were isolated, excised, fixed overnight with 4% paraformaldehyde and 20% sucrose, glued to a coverslip, and immunostained with VE-cadherin (1:100; Abcam) specific to ECs (40) for 1 hour at room temperature. Cy3-labeled secondary antibody (1:1,000; Abcam) was incubated at room temperature for 30 minutes, followed by DAPI staining (Thermo Fisher Scientific). After proper washes, tridimensional images and videos of longitudinal en face vessels were obtained by assembling 10 high-resolution images of multiple *z* stacks taken with a Nikon A1 scanning confocal microscope (Nikon Instruments) and acquired with NIS-Elements (Nikon Instruments) advanced research software. Images were optimized for contrast, without any further manipulation. Quantification of the endothelial coverage was performed by counting the red areas (VE-cadherin staining) of the central portion of the artery using ImageJ64 software. A schematic representation of the procedure is shown in Supplemental Figure 7A.

For the cross-section images, the arteries were excised as described above and embedded in OCT medium (Sakura Finetek USA) for cryosectioning. Subsequently, 10-μm sections were cut every 20 μm and submitted in toto for histological evaluation. Sections were processed for staining with the following antibodies: anti–α-SMA (Cy3-conjugated α-SMA, 1:1,000 for 3 hours at room temperature; Sigma-Aldrich), anti–VE-cadherin (1:100 overnight at 4°C; Abcam), and anti-GFP (1:1,000 overnight at 4°C; Thermo Fisher Scientific). Fluorescent-labeled secondary antibodies (1:1,000; Thermo Fisher Scientific) were incubated at room temperature for 1 hour (Alexa Fluor 488 was used for VE-cadherin detection and Cy3 for GFP detection). Samples were then washed with PBS and mounted with SlowFade Gold antifade reagent with DAPI (Thermo Fisher Scientific). Neointima/media ratios were calculated using ImageJ64 software as previously described (34). Cross-section images were acquired with a Nikon A1 scanning confocal microscope, and the number of VE-cadherin–positive cells in the circumference lumen was quantified.

Scanning electron microscopy. Longitudinal en face vascular preparations were fixed with 2.5% glutaraldehyde and 2 mM $CaCl_2$ in 75 mM Na-cacodylate buffer for at least 30 minutes. The tissues were rinsed in the buffer and washed in water for 15 minutes 3 times and subjected to a freeze-dry procedure: each vessel was plunged into precooled ethane, transferred into liquid nitrogen, slowly dried for 20 hours in a chamber (Leica EM AFS) in the presence of vapor-phase liquid nitrogen, and subjected to critical-point drying. The dried tissue was coated with a thin gold palladium layer using an ion spatter (Denton Desk IV Coater, Denton Vacuum) and examined under a scanning electron microscope (LEO 1550; Carl Zeiss) with a field-emission electron gun and SmartSEM version 5 software.

Vascular reactivity. Two and 4 weeks after injury, the rats were euthanized, and the common carotid arteries were quickly harvested and suspended in isolated tissue baths filled with 25 ml Krebs-Henseleit solution (118.3 mM NaCl, 4.7 mM KCl, 2.5 mM $CaCl_2$, 1.2 mM $MgSO_4$, 1.2 mM KH_2PO_4, 25 mM $NaHCO_3$, and 5.6 mM glucose) continuously bubbled with a mixture of 5% CO_2 and 95% O_2 (pH 7.38–7.42) at 37°C as previously described (65). Endothelium-dependent vasorelaxation was assessed in vessels preconstricted with phenylephrine (10^{-5} M) in response to acetylcholine from 10^{-9} to 10^{-6} M, as previously described (20, 64). Nitroprusside (from 10^{-9} to 10^{-6} M) was used to evaluate the endothelium-independent response (20). All drugs were freshly prepared on the day of the experiment. Concentrations are reported as the final molar value in the organ bath.

Statistics. Data are expressed as the mean ± SEM. One- or 2-way ANOVA was performed, as appropriate, with Tukey-Kramer's post hoc correction. All analyses were performed using GraphPad Prism 5.0 software. Specific tests and significance levels are reported in the figure legends. $P < 0.05$ was considered statistically significant.

Study approval. The IACUC of Columbia University Medical Center approved all animal study procedures. Human venous whole blood samples for the platelet adhesion assay were obtained from volunteers who provided signed, informed consent, according to Columbia University IRB protocols and Declaration of Helsinki principles.

Address correspondence to: Hana Totary-Jain, University of South Florida, Morsani College of Medicine, Department of Molecular Pharmacology and Physiology, 12901 Bruce B. Downs Blvd., MDC08, Tampa, Florida 33612, USA. Phone: 813.974.6821; E-mail: totaryjainh@health.usf.edu.

1. Stefanini GG, Holmes DR, Holmes DR Jr. Drug-eluting coronary-artery stents. *N Engl J Med*. 2013;368(3):254–265.

2. Nabel EG, Braunwald E. A tale of coronary artery disease and myocardial infarction. *N Engl J Med*. 2012;366(1):54–63.

3. De Luca G, et al. Drug-eluting vs bare-metal stents in primary angioplasty: a pooled patient-level meta-analysis of randomized trials. *Arch Intern Med*. 2012;172(8):611–621.

4. Chaabane C, Otsuka F, Virmani R, Bochaton-Piallat ML. Biological responses in stented arteries. *Cardiovasc Res*. 2013;99(2):353–363.

5. Marx SO, Totary-Jain H, Marks AR. Vascular smooth muscle cell proliferation in restenosis. *Circ Cardiovasc Interv*. 2011;4(1):104–111.

6. Santulli G, Totary-Jain H. Tailoring mTOR-based therapy: molecular evidence and clinical challenges. *Pharmacogenomics*. 2013;14(12):1517–1526.

7. Totary-Jain H, Sanoudou D, Dautriche CN, Schneller H, Zambrana L, Marks AR. Rapamycin resistance is linked to defective regulation of Skp2. *Cancer Res*. 2012;72(7):1836–1843.

8. Sun J, Marx SO, Chen HJ, Poon M, Marks AR, Rabbani LE. Role for p27(Kip1) in Vascular Smooth Muscle Cell Migration. *Circulation*. 2001;103(24):2967–2972.

9. Marx SO, Jayaraman T, Go LO, Marks AR. Rapamycin-FKBP inhibits cell cycle regulators of proliferation in vascular smooth muscle cells. *Circ Res*. 1995;76(3):412–417.

10. Marks AR. Sirolimus for the prevention of in-stent restenosis in a coronary artery. *N Engl J Med*. 2003;349(14):1307–1309.

11. Joner M, et al. Endothelial cell recovery between comparator polymer-based drug-eluting stents. *J Am Coll Cardiol*. 2008;52(5):333–342.

12. Guagliumi G, et al. Examination of the in vivo mechanisms of late drug-eluting stent thrombosis: findings from optical coherence tomography and intravascular ultrasound imaging. *JACC Cardiovasc Interv*. 2012;5(1):12–20.

13. Liu HT, et al. Rapamycin inhibits re-endothelialization after percutaneous coronary intervention by impeding the proliferation and migration of endothelial cells and inducing apoptosis of endothelial progenitor cells. *Tex Heart Inst J*. 2010;37(2):194–201.

14. Cassese S, Kastrati A. New-generation drug-eluting stents for patients with myocardial infarction. *JAMA*. 2012;308(8):814–815.

15. Otsuka F, Finn AV, Yazdani SK, Nakano M, Kolodgie FD, Virmani R. The importance of the endothelium in atherothrombosis and coronary stenting. *Nat Rev Cardiol*. 2012;9(8):439–453.

16. Otsuka F, et al. Pathology of second-generation everolimus-eluting stents versus first-generation sirolimus- and Paclitaxel-eluting stents in humans. *Circulation*. 2014;129(2):211–223.

17. Daemen J, et al. Early and late coronary stent thrombosis of sirolimus-eluting and paclitaxel-eluting stents in routine clinical practice: data from a large two-institutional cohort study. *Lancet*. 2007;369(9562):667–678.

18. Ali ZA, et al. Increased thin-cap neoatheroma and periprocedural myocardial infarction in drug-eluting stent restenosis: multimodality intravascular imaging of drug-eluting and bare-metal stents. *Circ Cardiovasc Interv*. 2013;6(5):507–517.

19. Joner M, et al. Pathology of drug-eluting stents in humans: delayed healing and late thrombotic risk. *J Am Coll Cardiol*. 2006;48(1):193–202.

20. Santulli G, et al. CaMK4 Gene Deletion Induces Hypertension. *J Am Heart Assoc*. 2012;1(4):e001081.

21. Finn AV, Vorpahl M, Ladich E, Virmani R. Future directions in stenting. *Expert Rev Cardiovasc Ther*. 2010;8(1):1–6.

22. Elia L, et al. The knockout of miR-143 and -145 alters smooth muscle cell maintenance and vascular homeostasis in mice: correlates with human disease. *Cell Death Differ*. 2009;16(12):1590–1598.

23. Cordes KR, et al. miR-145 and miR-143 regulate smooth muscle cell fate and plasticity. *Nature*. 2009;460(7256):705–710.

24. McDonald RA, et al. miRNA-21 is dysregulated in response to vein grafting in multiple models and genetic ablation in mice attenuates neointima formation. *Eur Heart J*. 2013;34(22):1636–1643.

25. Wang S, et al. The endothelial-specific microRNA miR-126 governs vascular integrity and angiogenesis. *Dev Cell*. 2008;15(2):261–271.

26. Schober A, et al. MicroRNA-126-5p promotes endothelial proliferation and limits atherosclerosis by suppressing Dlk1. *Nat Med*. 2014;20(4):368–376.

27. Nichol D, Stuhlmann H. EGFL7: a unique angiogenic signaling factor in vascular development and disease. *Blood*. 2012;119(6):1345–1352.

28. Brown BD, Venneri MA, Zingale A, Sergi Sergi L, Naldini L. Endogenous microRNA regulation suppresses transgene expression in hematopoietic lineages and enables stable gene transfer. *Nat Med*. 2006;12(5):585–591.

29. Qiao C, et al. Liver-specific microRNA-122 target sequences incorporated in AAV vectors efficiently inhibits transgene expression in the liver. *Gene Ther*. 2011;18(4):403–410.

30. Fish JE, et al. miR-126 regulates angiogenic signaling and vascular integrity. *Dev Cell*. 2008;15(2):272–284.

31. Kelly EJ, Hadac EM, Greiner S, Russell SJ. Engineering microRNA responsiveness to decrease virus pathogenicity. *Nat Med*. 2008;14(11):1278–1283.

32. Brown BD, Naldini L. Exploiting and antagonizing microRNA regulation for therapeutic and experimental applications. *Nat Rev Genet*. 2009;10(8):578–585.

33. Haraguchi T, Ozaki Y, Iba H. Vectors expressing efficient RNA decoys achieve the long-term suppression of specific microRNA activity in mammalian cells. *Nucleic Acids Res*. 2009;37(6):e43.

34. Iaccarino G, Smithwick LA, Lefkowitz RJ, Koch WJ. Targeting Gβγ signaling in arterial vascular smooth muscle proliferation: a novel strategy to limit restenosis. *Proc Natl Acad Sci U S A*. 1999;96(7):3945–3950.

35. Sorriento D, Santulli G, Fusco A, Anastasio A, Trimarco B, Iaccarino G. Intracardiac injection of AdGRK5-NT reduces left ventricular hypertrophy by inhibiting NF-κB-dependent hypertrophic gene expression. *Hypertension*. 2010;56(4):696–704.

36. Chen D, Krasinski K, Sylvester A, Chen J, Nisen PD, Andres V. Downregulation of cyclin-dependent kinase 2 activity and cyclin A promoter activity in vascular smooth muscle cells by p27(KIP1), an inhibitor of neointima formation in the rat carotid artery. *J Clin Invest*. 1997;99(10):2334–2341.

37. Tanner FC, et al. Differential effects of the cyclin-dependent kinase inhibitors p27(Kip1), p21(Cip1), and p16(Ink4) on vascular smooth muscle cell proliferation. *Circulation*. 2000;101(17):2022–2025.

38. Moss SC, Lightell DJ, Lightell DJ Jr, Marx SO, Marks AR, Woods TC. Rapamycin regulates endothelial cell migration through regulation of the cyclin-dependent kinase inhibitor p27Kip1. *J Biol Chem*. 2010;285(16):11991–11997.

39. Goukassian D, et al. Overexpression of p27(Kip1) by doxycycline-regulated adenoviral vectors inhibits endothelial cell proliferation and migration and impairs angiogenesis. *FASEB J*. 2001;15(11):1877–1885.

40. Vestweber D. VE-cadherin: the major endothelial adhesion molecule controlling cellular junctions and blood vessel formation. *Arterioscler Thromb Vasc Biol*. 2008;28(2):223–232.

41. Park SJ, Kang SJ, Virmani R, Nakano M, Ueda Y. In-stent neoatherosclerosis: a final common pathway of late stent failure. *J Am Coll Cardiol*. 2012;59(23):2051–2057.

42. Zhou J, et al. Regulation of vascular smooth muscle cell turnover by endothelial cell-secreted microRNA-126: role of shear stress. *Circ Res*. 2013;113(1):40–51.

43. Gonzalez P, et al. A single-nucleotide polymorphism in the human p27kip1 gene (−838C>A) affects basal promoter activity and the risk of myocardial infarction. *BMC Biol*. 2004;2:5.

44. Boehm M, et al. Bone marrow-derived immune cells regulate vascular disease through a p27(Kip1)-dependent mechanism. *J Clin Invest*. 2004;114(3):419–426.

45. Luscher TF, et al. Drug-eluting stent and coronary thrombosis: biological mechanisms and clinical implications. *Circulation*. 2007;115(8):1051–1058.

46. Farb A, Burke AP, Kolodgie FD, Virmani R. Pathological mechanisms of fatal late coronary stent thrombosis in humans. *Circulation*. 2003;108(14):1701–1706.

47. Padfield GJ, Newby DE, Mills NL. Understanding the role of endothelial progenitor cells in percutaneous coronary intervention. *J Am Coll Cardiol*. 2010;55(15):1553–1565.

48. Rossi ML, Zavalloni D, Gasparini GL, Mango R, Belli G, Presbitero P. The first report of late stent thrombosis leading to acute myocardial infarction in patient receiving the new endothelial progenitor cell capture stent. *Int J Cardiol*. 2010;141(1):e20–e22.

49. Akyurek LM, Boehm M, Olive M, Zhou AX, San H, Nabel EG. Deficiency of cyclin-dependent kinase inhibitors p21Cip1 and p27Kip1 accelerates atherogenesis in apolipoprotein E-deficient mice. *Biochem Biophys Res Commun*. 2010;396(2):359–363.

50. Indolfi C, et al. Activation of cAMP-PKA signaling in vivo inhibits smooth muscle cell pro-

liferation induced by vascular injury. *Nat Med*. 1997;3(7):775–779.

51. Claudio PP, et al. Adenoviral RB2/p130 gene transfer inhibits smooth muscle cell proliferation and prevents restenosis after angioplasty. *Circ Res*. 1999;85(11):1032–1039.

52. Luo Z, Sata M, Nguyen T, Kaplan JM, Akita GY, Walsh K. Adenovirus-mediated delivery of fas ligand inhibits intimal hyperplasia after balloon injury in immunologically primed animals. *Circulation*. 1999;99(14):1776–1779.

53. Lamfers ML, et al. In vivo suppression of restenosis in balloon-injured rat carotid artery by adenovirus-mediated gene transfer of the cell surface-directed plasmin inhibitor ATF.BPTI. *Gene Ther*. 2001;8(7):534–541.

54. Virmani R, Kolodgie FD, Farb A, Lafont A. Drug eluting stents: are human and animal studies comparable? *Heart*. 2003;89(2):133–138.

55. Kolandaivelu K, Leiden BB, Edelman ER. Predicting response to endovascular therapies: Dissecting the roles of local lesion complexity, systemic comorbidity, and clinical uncertainty. *J Biomech*. 2014;47(4):908–921.

56. Kang SH, et al. Biodegradable-polymer drug-eluting stents vs. bare metal stents vs. durable-polymer drug-eluting stents: a systematic review and Bayesian approach network meta-analysis. *Eur Heart J*. 2014;35(17):1147–1158.

57. Ebert MS, Neilson JR, Sharp PA. MicroRNA sponges: competitive inhibitors of small RNAs in mammalian cells. *Nat Methods*. 2007; 4(9):721–726.

58. Iaccarino G, et al. Ischemic neoangiogenesis enhanced by beta2-adrenergic receptor overexpression: a novel role for the endothelial adrenergic system. *Circ Res*. 2005;97(11):1182–1189.

59. Totary-Jain H, et al. Reprogramming of the microRNA transcriptome mediates resistance to rapamycin. *J Biol Chem*. 2013; 288(9):6034–6044.

60. Ciccarelli M, et al. Endothelial α1-adrenoceptors regulate neo-angiogenesis. *Br J Pharmacol*. 2008;153(5):936–946.

61. Sorriento D, et al. The G-protein-coupled receptor kinase 5 inhibits NFκB transcriptional activity by inducing nuclear accumulation of IκB α. *Proc Natl Acad Sci U S A*. 2008;105(46):17818–17823.

62. Santulli G, et al. Evaluation of the anti-angiogenic properties of the new selective αVβ3 integrin antagonist RGDechiHCit. *J Transl Med*. 2011;9:7.

63. Doggett TA, et al. Selectin-like kinetics and biomechanics promote rapid platelet adhesion in flow: the GPIb(α)-vWF tether bond. *Biophys J*. 2002;83(1):194–205.

64. Iaccarino G, et al. AKT participates in endothelial dysfunction in hypertension. *Circulation*. 2004;109(21):2587–2593.

65. Santulli G, et al. In vivo properties of the proangiogenic peptide QK. *J Transl Med*. 2009;7:41.

ONLINE DATA SUPPLEMENTS

Santulli G. et al. **"A microRNA-based strategy to suppress restenosis while preserving endothelial function"**

**Supplementary Figures**

Figure S1
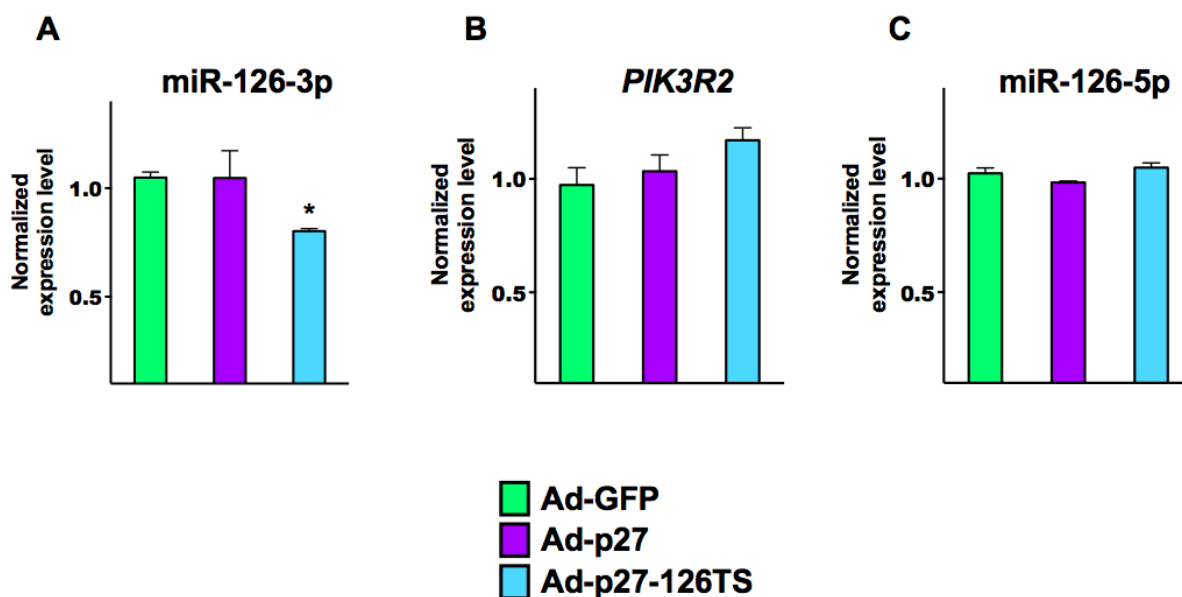
Effect of Ad-p27-126TS on the expression of miR-126-3p, *PIK3R2* and miR-126-5p in vitro.
EC were infected with the indicated adenoviruses for 24 h. Total RNA was extracted, and real time RT-qPCR for 126-3p **(A)**, *PIK3R2* **(B)**, and miR-126-5p **(C)** was performed. Expression levels of miRNAs were normalized to U18, *PIK3R2* was normalized to *GAPDH*. Data shown are means±SE; *$p < 0.05$ vs Ad-GFP, one-way ANOVA, Tukey-Kramer *post hoc* test.

Figure S2
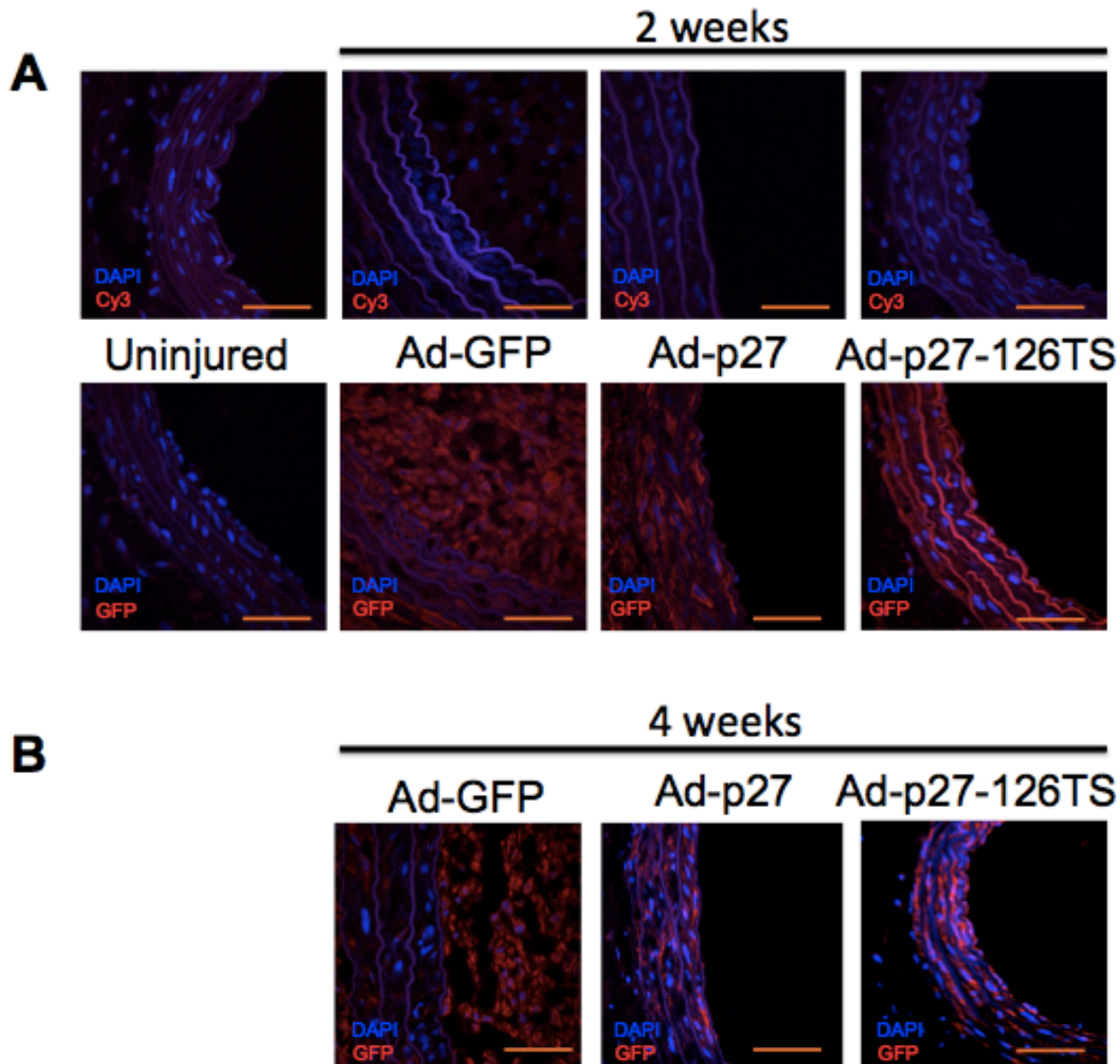
Efficiency of Ad infection two and four weeks after surgery.
The efficiency of Ad infection was evaluated 2 (**A**) and 4 weeks after surgery (**B**) using a primary antibody against GFP detected using a Cy3-coniugated secondary antibody. Representative digital images are shown. In A, top: negative control (secondary antibody alone, Cy3); bottom: staining for GFP revealed by Cy3. Scale bar represents 100 µm (magnification 60×).

Figure S3
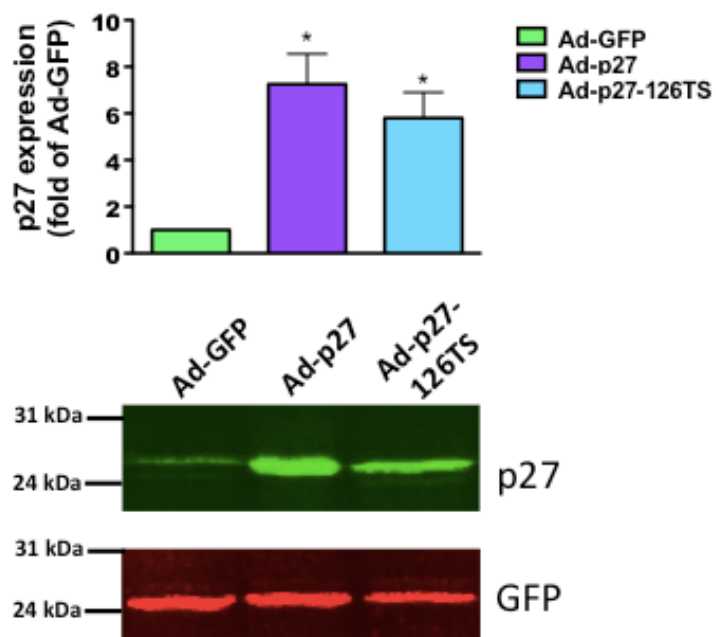
Assessment of p27 overexpression in the carotid wall three days after surgery. Three days after infection with the indicated Ad constructs the vessels were homogenized and samples were size-fractionated by SDS-PAGE; proteins were transferred to polyvinylidene difluoride membrane and visualized by immunoblotting using infrared-labeled antibodies. Data shown in the graph represents means±SE; *p<0.05 vs Ad-GFP, one-way ANOVA, Tukey-Kramer *post hoc* test.

Figure S4
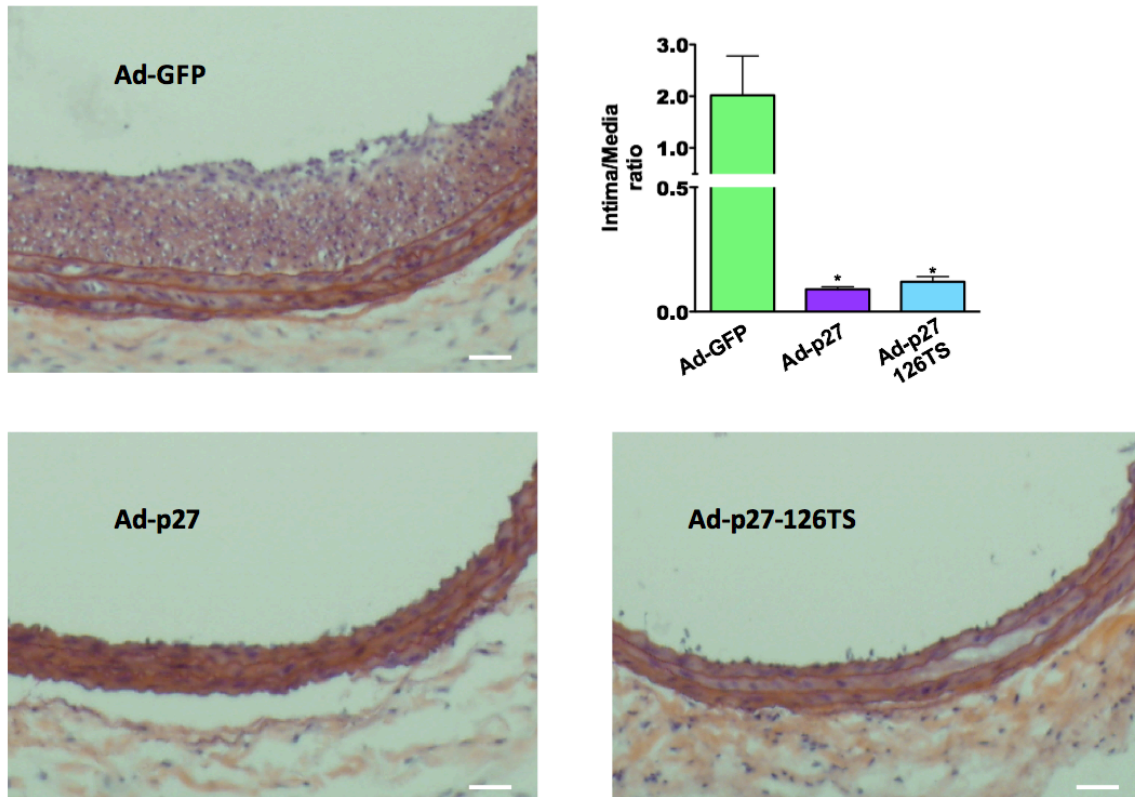
Ad-p27 and Ad-p27-126TS inhibit restenosis 4 weeks after balloon injury.
Representative sections stained with hematoxylin / eosin (magnification 40×; dimensional bar represents 100 µm). Intima/media ratios were calculated from at least 6 rats/group. All data shown are means ± SEM. Data comparisons were made using one way ANOVA followed by Tukey-Kramer *post hoc* test; *$P<0.01$ versus Ad-GFP.

Figure S5

A
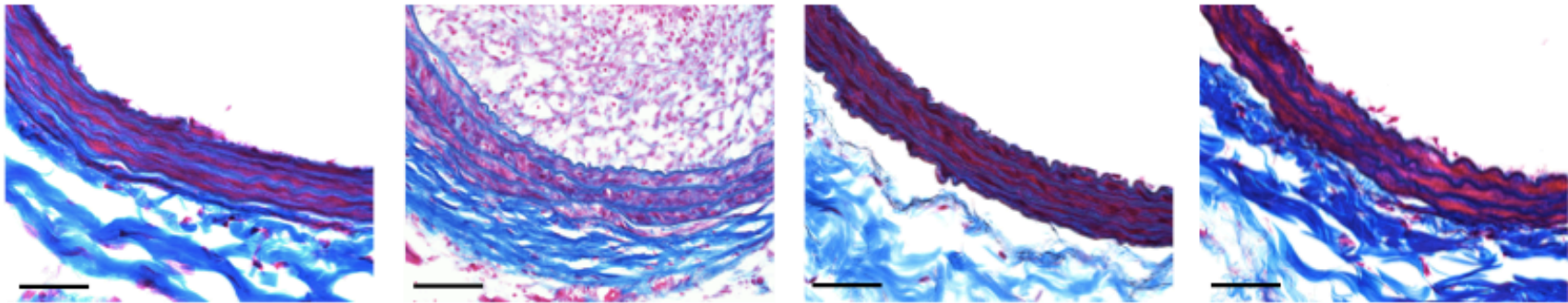
| Uninjured | Ad-GFP | Ad-p27 | Ad-p27-126TS |

B
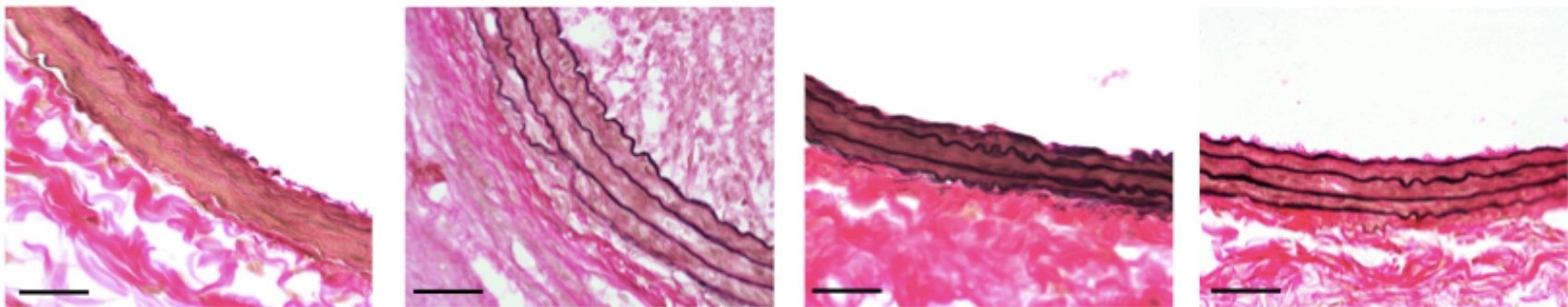
Ad-p27 and Ad-p27-126TS restored the arterial structure to the uninjured control vessel.
Representative sections stained with **(A)** Masson's Trichrome to detect collagen fibers or **(B)** Verhoeff Van Gieson to detect elastin fibers (magnification 40×; dimensional bar represents 100 μm).

Figure S6.
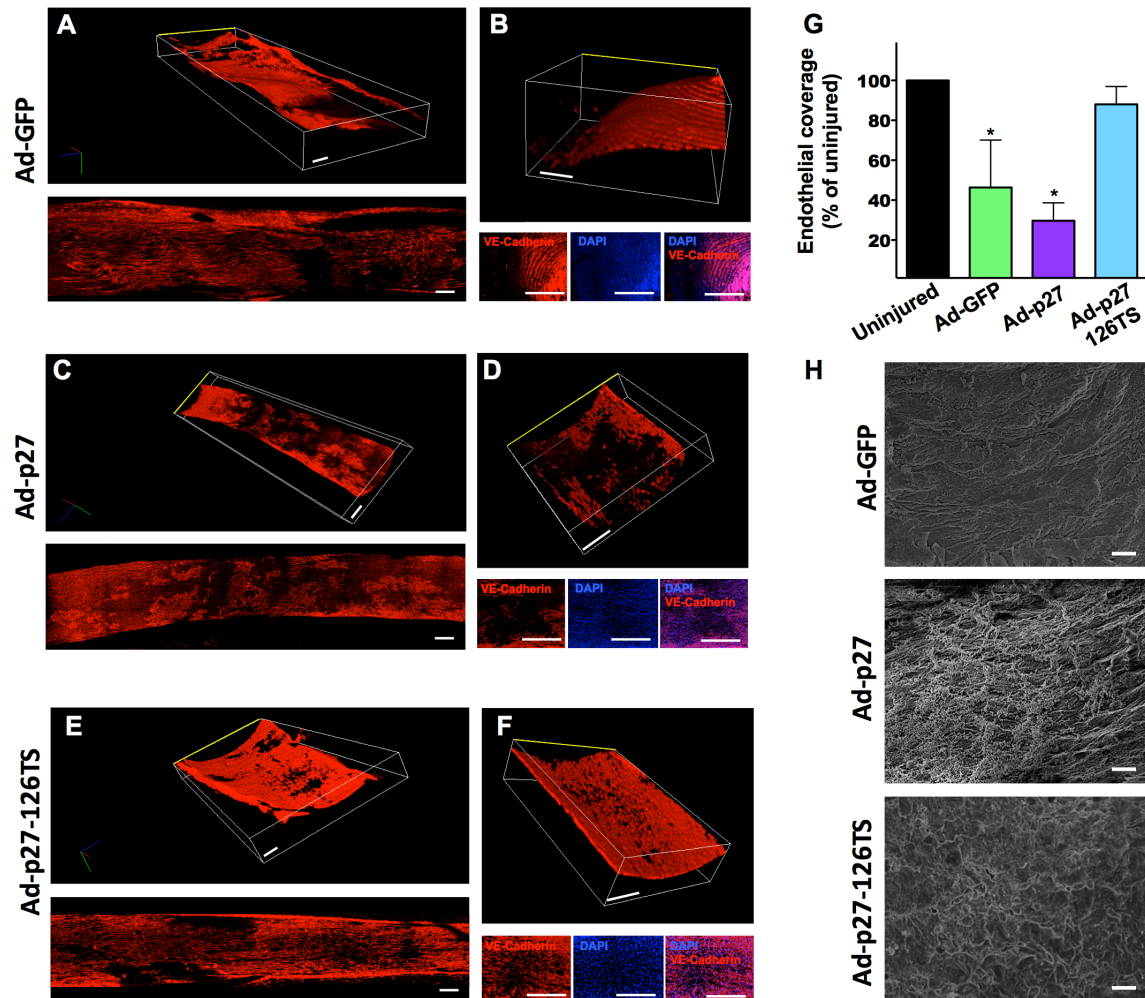
Endothelial coverage assessed by confocal electron microscopy of *en face* longitudinal arterial preparations 4 weeks after injury.

(**A-F**) Representative confocal images of the internal surface of the vessels immunostained for VE-Cadherin acquired at the. (**A, C, E**) Tridimensional (top) and bidimensional (bottom) imaging of the longitudinal *en face* preparation of the carotid arteries. (**B, D, F**) Tridimensional imaging of a representative central portion (see the methods and **Supplementary Fig. 7A** for detailed information about the imaging procedure) of the vessel (top), with the respective 2D

pictures showing the EC-specific immunostaining for VE-cadherin (bottom: VE-cadherin, DAPI and merge, as indicated), representing the endothelial coverage, which is quantified in panel **G**; the luminal side is indicated by the yellow line; see also the **Supplementary videos 5-7** for a tridimensional view. In all 2D and 3D pictures the dimensional bar is 400 µm. All data shown are means ± SEM. Data comparisons were made using one-way ANOVA with Tukey-Kramer *post hoc* test; n = at least 5/group; *$P<0.01$ versus uninjured. (**H**) Representative scanning electron microscopy (SEM) images of the internal surface of uninjured, Ad-GFP, Ad-p27 and Ad-p27-126TS infected arteries. In SEM pictures, the scale bar indicates 10 µm.

Figure S7

A

B

C

Cy3   DAPI   DAPI Cy3
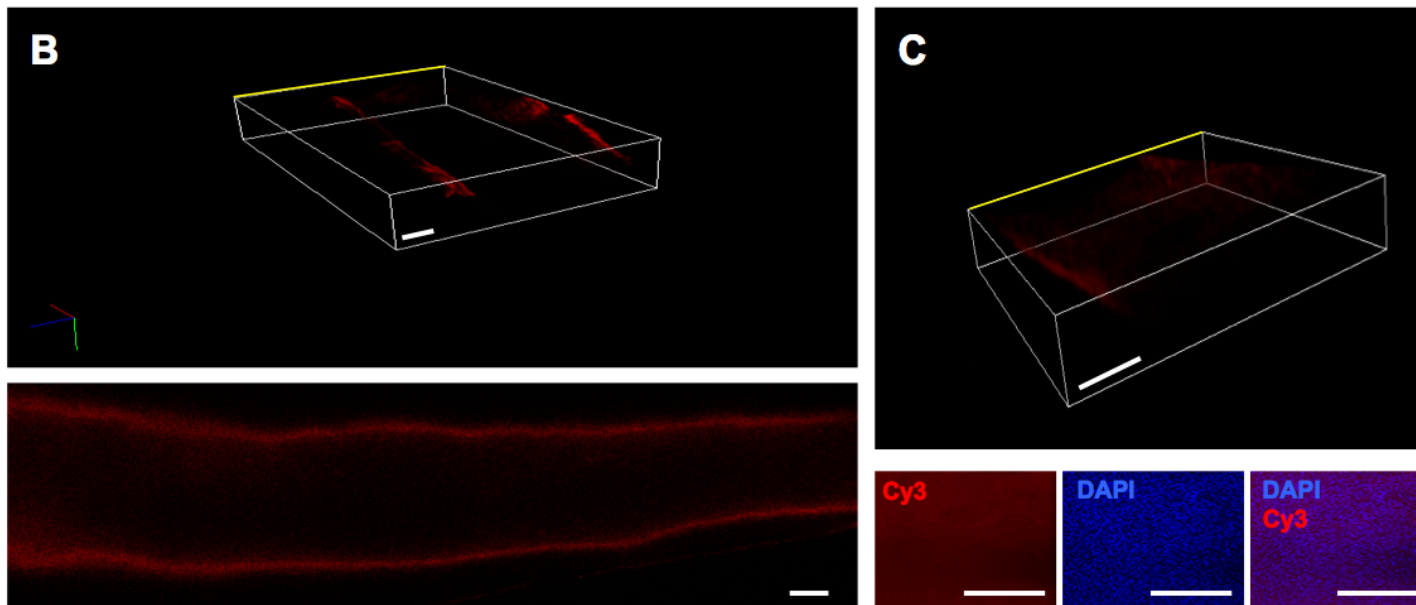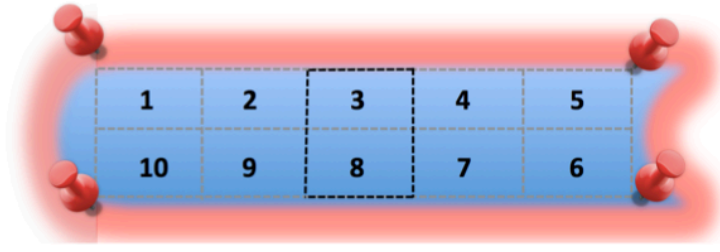
Imaging and quantifications of the longitudinal *en face* arterial preparations.
(**A**) Schematic representation of the examination of en face preparations at the confocal microscope. Ten adjacent quadrants of each carotid artery were independently scanned and subsequently 3D reconstructed using a dedicated software (Nikon NIS-Elements) to obtain the image of the whole vessel. The quantification of the endothelial coverage (VE-Cadherin staining) was performed quantifying the red areas of the central portion of the artery (represented by bold dashed lines, quadrants 3 and 8) by using ImageJ64. (**B**) No specific staining is shown (20× magnification, confocal microscope) in the whole uninjured vessel stained with the Cy3 secondary antibody alone. Tridimensional (top) and bi-dimensional (bottom) imaging of the longitudinal *en face* preparation of the carotid artery is depicted. (**C**) Tridimensional

imaging (top) of a representative central portion of the vessel, with the respective 2D pictures (bottom) showing the immunostaining for Cy3, DAPI and merge, as indicated. See the **supplementary video 8 A and B** relative to the 3D images of the samples. Scale bar: 400 μm.

Figure S8
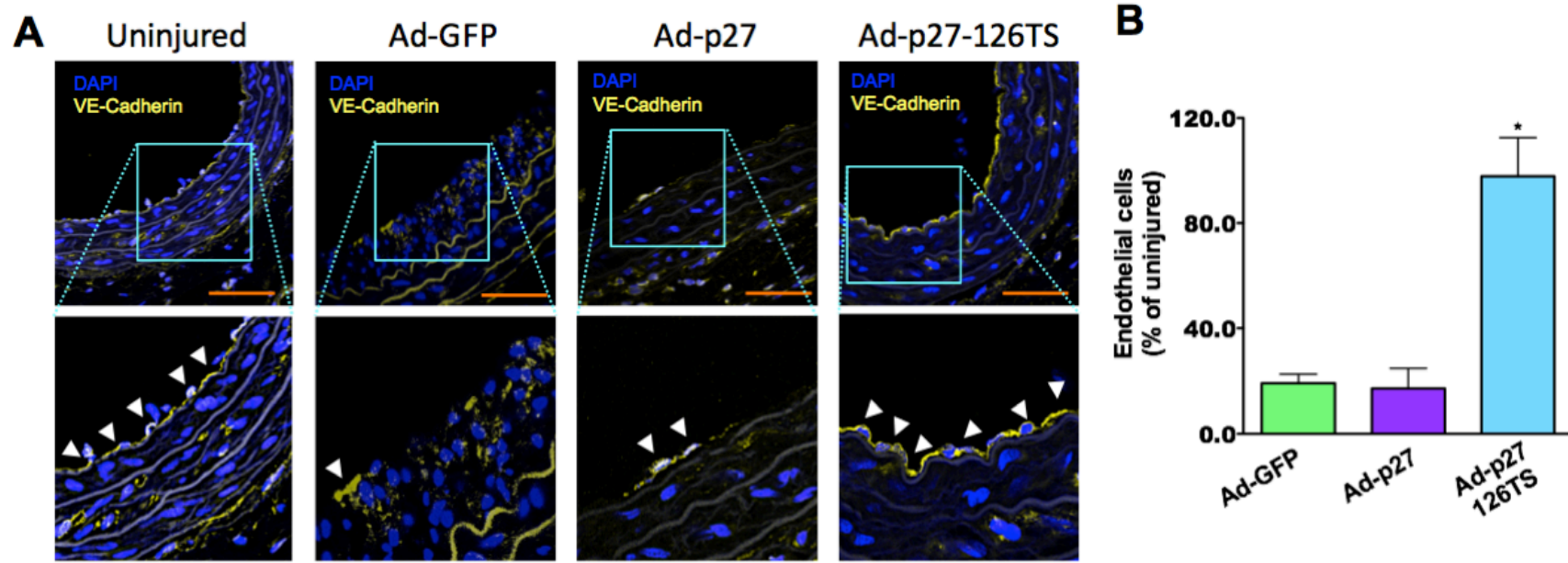
Ad-p27-126TS restores re-endothelialization in cross sections of injured carotid arteries.

(**A**) Representative sections of rat carotid arteries immunostained for the specific EC marker VE-Cadherin 4 weeks after injury. Nuclei were counterstained with DAPI. Orange scale bars: 100 μm (magnification 60×, inlays show high magnification images), arrowheads indicate EC beyond the inner autofluorescent elastic laminae. (**B**) Quantification of endothelial coverage was performed by counting the number of VE-cadherin positive cells in the circumference lumen from 6 sections/group. All data shown are means ± SEM. Data comparison was performed using one-way ANOVA, Tukey-Kramer *post hoc* test.

Figure S9

Uninjured

Ad-GFP   Ad-p27   Ad-p27-126TS
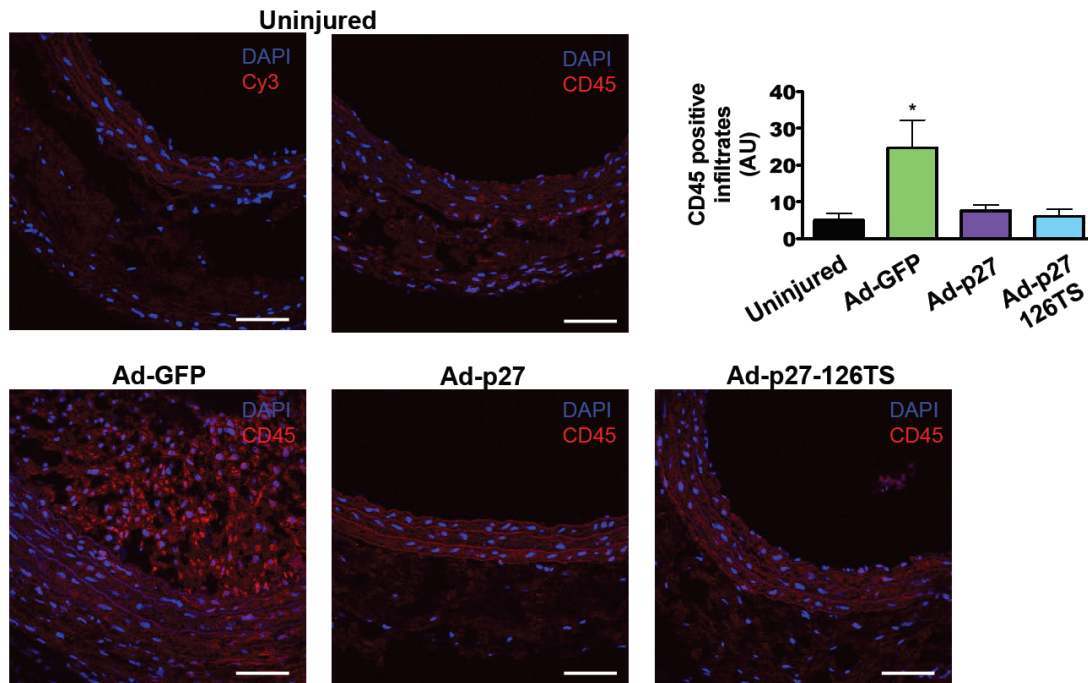
Ad-p27 and Ad-p27-126TS inhibit arterial inflammation 2 weeks after balloon injury.

Representative sections of rat carotid arteries immunostained for CD45, 2 weeks after injury. Nuclei were counterstained with DAPI. No positive staining was observed in the negative control sections (Cy3 alone). White scale bars: 100 μm (magnification 40×). CD45 positive cells were quantified by counting the number of CD45 positive cells in the intimal and medial areas from at least 3 sections/group. Data comparison was made using one way ANOVA, Tukey-Kramer *post hoc* test; *$P<0.05$ versus uninjured.

Figure S10
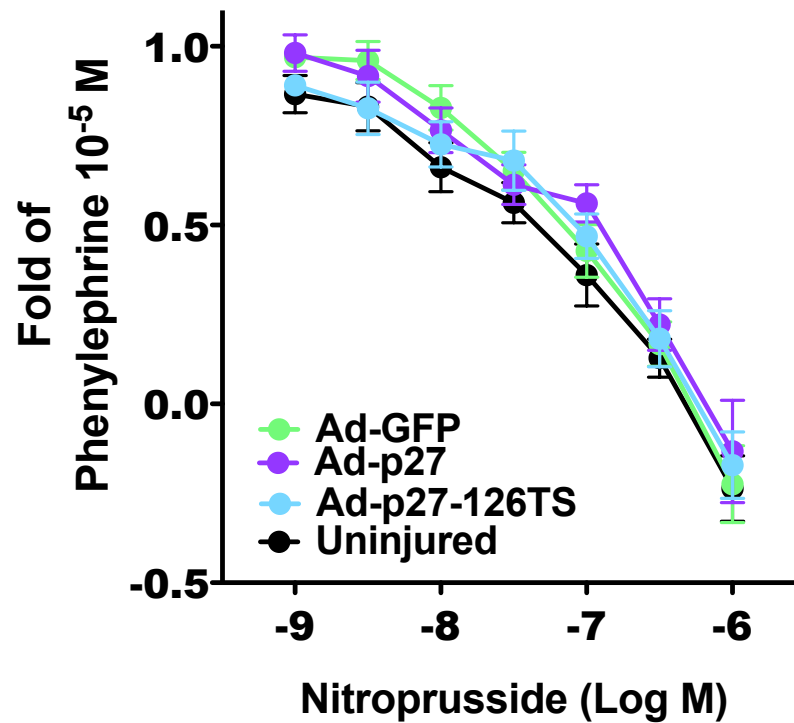
Vasodilatory response of carotid arteries to nitroprusside.
Carotid rings 2 weeks after injury showing the vasodilatative response to nitroprusside. n=5-6 rats/group. All the data are means ± SEM.

Video Legends

Supplementary Video 1
Uninjured vessel.
This video refers to Figure **4AB**. Representative tridimensional reconstruction of a longitudinal *en face* preparation (**A**) of an **uninjured** rat carotid artery immunostained with VE-cadherin (revealed by a Cy3 conjugated secondary antibody) and acquired at the confocal microscopy after assembling distinct portions of the vessel [the acquisition of the central portion of the artery is shown in **B**] each obtained from a high resolution focal stack of 2D images using sequential refocusing. In **B**, the EC-specific immunostaining for VE-cadherin of a central portion of the vessel is shown in red (Cy3), followed by DAPI staining and then the merge (Cy3/DAPI).

Supplementary Video 2
Ad-GFP infected rat carotid artery two weeks after injury.
This video refers to Figure **4 CD**. Representative tridimensional reconstruction of a longitudinal *en face* preparation (**C**) of an **Ad-GFP** infected rat carotid artery **two weeks** after injury immunostained with VE-cadherin (revealed by a Cy3 conjugated secondary antibody) and acquired at the confocal microscopy after assembling distinct portions of the vessel [the acquisition of the central portion of the artery is shown in **D**] each obtained from a high resolution focal stack of 2D images using sequential refocusing. In **D**, the EC-specific immunostaining for VE-cadherin of a central portion of the vessel is shown in red (Cy3), followed by DAPI staining and then the merge (Cy3/DAPI).

Supplementary Video 3
Ad-p27 infected rat carotid artery two weeks after injury.
This video refers to Figure **4 EF**. Representative tridimensional reconstruction of a longitudinal *en face* preparation (**E**) of an **Ad-p27** infected rat carotid artery **two weeks** after injury immunostained with VE-cadherin (revealed by a Cy3 conjugated secondary antibody) and acquired at the confocal microscopy after assembling distinct portions of the vessel [the acquisition of the central portion of the artery is shown in **F**] each obtained from a high resolution focal stack of 2D images using sequential refocusing. In **F**, the EC-specific immunostaining for VE-cadherin of a central portion of the vessel is shown in red (Cy3), followed by DAPI staining and then the merge (Cy3/DAPI).

Supplementary Video 4
Ad-p27-126TS infected rat carotid artery two weeks after injury.
This video refers to Figure **4 GH**. Representative tridimensional reconstruction of a longitudinal *en face* preparation (**G**) of an **Ad-p27-126TS** infected rat carotid artery **two weeks** after injury immunostained with VE-cadherin (revealed by a Cy3 conjugated secondary antibody) and acquired at the confocal microscopy after assembling distinct portions of the vessel [the acquisition of the central portion of the artery is shown in **H**] each obtained from a high resolution focal

stack of 2D images using sequential refocusing. In **H**, the EC-specific immunostaining for VE-cadherin of a central portion of the vessel is shown in red (Cy3), followed by DAPI staining and then the merge (Cy3/DAPI).

Supplementary Video 5
Ad-GFP infected rat carotid artery four weeks after injury.
This video refers to Figure **S5 AB**. Representative tridimensional reconstruction of a longitudinal *en face* preparation (**A**) of an **Ad-GFP** infected rat carotid artery **four weeks** after injury immunostained with VE-cadherin (revealed by a Cy3 conjugated secondary antibody) and acquired at the confocal microscopy after assembling distinct portions of the vessel [the acquisition of the central portion of the artery is shown in **B**] each obtained from a high resolution focal stack of 2D images using sequential refocusing. In **B**, the EC-specific immunostaining for VE-cadherin of a central portion of the vessel is shown in red (Cy3), followed by DAPI staining and then the merge (Cy3/DAPI).

Supplementary Video 6
Ad-p27 infected rat carotid artery four weeks after injury.
This video refers to Figure **S5 CD**. Representative tridimensional reconstruction of a longitudinal *en face* preparation (**C**) of an **Ad-p27** infected rat carotid artery **four weeks** after injury immunostained with VE-cadherin (revealed by a Cy3 conjugated secondary antibody) and acquired at the confocal microscopy after assembling distinct portions of the vessel [the acquisition of the central portion of the artery is shown in **D**] each obtained from a high resolution focal stack of 2D images using sequential refocusing. In **D**, the EC-specific immunostaining for VE-cadherin of a central portion of the vessel is shown in red (Cy3), followed by DAPI staining and then the merge (Cy3/DAPI).

Supplementary Video 7
Ad-p27-126TS infected rat carotid artery four weeks after injury.
This video refers to Figure **S5 EF**. Representative tridimensional reconstruction of a longitudinal *en face* preparation (**E**) of an **Ad-p27-126TS** infected rat carotid artery **four weeks** after injury immunostained with VE-cadherin (revealed by a Cy3 conjugated secondary antibody) and acquired at the confocal microscopy after assembling distinct portions of the vessel [the acquisition of the central portion of the artery is shown in **F**] each obtained from a high resolution focal stack of 2D images using sequential refocusing. In **F**, the EC-specific immunostaining for VE-cadherin of a central portion of the vessel is shown in red (Cy3), followed by DAPI staining and then the merge (Cy3/DAPI).

Supplementary Video 8
Negative control (Secondary antibody alone).
This video refers to Figure **S7B and C**. Representative tridimensional reconstruction of a longitudinal *en face* preparation of an uninjured rat carotid artery (stained with a Cy3 conjugated secondary antibody alone, as **negative control**) and acquired at the confocal microscopy after assembling distinct

portions of the vessel [the acquisition of the central portion of the artery is shown in **C**] each obtained from a high resolution focal stack of 2D images using sequential refocusing. In **C**, a central portion of the vessel incubated with the Cy3 conjugated secondary alone is shown, followed by DAPI and merge.